

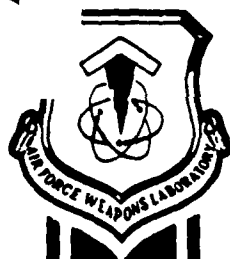
DTIC FILE COPY

AFWL-TR-88-114

AFWL-TR-
88-114

(2)

AD-A206 604



A
F
W
L

Sigma

CHARACTERIZATION OF CHEMICAL SOURCES OF $N_2(A^3\Sigma^+_U)$

Dr G. Black

SRI International
333 Ravenswood Ave
Menlo Park, CA 94025

February 1989

Final Report

Approved for public release; distribution unlimited.

AIR FORCE WEAPONS LABORATORY
Air Force Systems Command
Kirtland Air Force Base, NM 87117-6008

DTIC
ELECTE
APR 11 1989
S H D

This final report was prepared by SRI International, Menlo Park, Calif. under Contract F29601-84-C-0099, Job Order 33261W12 with the Air Force Weapons Laboratory, Kirtland Air Force Base, New Mexico. Capt Robert P. Crannage, Jr., AFWL/ARD was the Laboratory Project Officer-in-Charge.

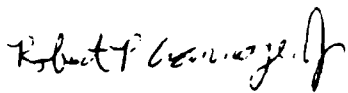
When Government drawings, specifications, or other data are used for any purpose other than in connection with a definitely Government-related procurement, the United States Government incurs no responsibility or any obligation whatsoever. The fact that the Government may have formulated or in any way supplied the said drawings, specifications, or other data, is not to be regarded by implication, or otherwise in any manner construed, as licensing the holder, or any other person or corporation; or as conveying any rights or permission to manufacture, use or sell any patented invention that may in any way be related thereto.

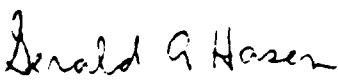
This report has been authored by a contractor of the United States Government. Accordingly, the United States Government retains a nonexclusive, royalty-free license to publish or reproduce the material contained herein, or allow others to do so, for the United States Government purposes.

This report has been reviewed by the Public Affairs Office and is releasable to the National Technical Information Service (NTIS). At NTIS, it will be available to the general public, including foreign nationals.

If your address has changed, if you wish to be removed from our mailing list, or if your organization no longer employs the addressee, please notify AFWL/ARD, Kirtland AFB, NM 87117-6008 to help us maintain a current mailing list.

This technical report has been reviewed and is approved for publication.


ROBERT P. CRANNAGE, JR.
Capt, USAF
Project Officer


GERALD A. HASEN
Lt Col, USAF
Chief, Advanced Chemical Laser Branch

FOR THE COMMANDER

ERIC J. JUMPER
Lt Col, USAF
Chief, Devices Division

DO NOT RETURN COPIES OF THIS REPORT UNLESS CONTRACTUAL OBLIGATIONS OR NOTICE ON A SPECIFIC DOCUMENT REQUIRES THAT IT BE RETURNED.

UNCLASSIFIED

SECURITY CLASSIFICATION OF THIS PAGE

REPORT DOCUMENTATION PAGE				Form Approved OMB No. 0704-0188	
1a. REPORT SECURITY CLASSIFICATION UNCLASSIFIED			1b. RESTRICTIVE MARKINGS		
2a. SECURITY CLASSIFICATION AUTHORITY			3. DISTRIBUTION/AVAILABILITY OF REPORT Approved for public release; distribution unlimited.		
2b. DECLASSIFICATION/DOWNGRADING SCHEDULE			5. MONITORING ORGANIZATION REPORT NUMBER(S) AFWL-TR-88-114		
4. PERFORMING ORGANIZATION REPORT NUMBER(S) MP-88-214			7a. NAME OF MONITORING ORGANIZATION Air Force Weapons Laboratory		
6a. NAME OF PERFORMING ORGANIZATION SRI International		6b. OFFICE SYMBOL (if applicable)		7b. ADDRESS (City, State, and ZIP Code) Kirtland Air Force Base, NM 87117-6008	
6c. ADDRESS (City, State, and ZIP Code) 333 Ravenswood Avenue Menlo Park, CA 94025			9. PROCUREMENT INSTRUMENT IDENTIFICATION NUMBER F29601-84-C-0099		
8a. NAME OF FUNDING/SPONSORING ORGANIZATION		8b. OFFICE SYMBOL (if applicable)		10. SOURCE OF FUNDING NUMBERS	
6c. ADDRESS (City, State, and ZIP Code)		PROGRAM ELEMENT NO. 62601F		PROJECT NO. 3326	TASK NO. 1W
				WORK UNIT ACCESSION NO. 12	
11. TITLE (Include Security Classification) CHARACTERIZATION OF CHEMICAL SOURCES OF $N_2(A^3\Sigma^+)$					
12. PERSONAL AUTHOR(S) Black, Graham Dr					
13a. TYPE OF REPORT Final		13b. TIME COVERED FROM Sep 84 TO Sep 88		14. DATE OF REPORT (Year, Month, Day) 1989 February	
				15. PAGE COUNT 80	
16. SUPPLEMENTARY NOTATION					
17. COSATI CODES			18. SUBJECT TERMS (Continue on reverse if necessary and identify by block number)		
FIELD	GROUP	SUB-GROUP	Nitrogen)		
07	05		Chemiluminescence)		
07	02		Resonance-Enhanced, Multiphoton Ionization Technique. (Sign)		
19. ABSTRACT (Continue on reverse if necessary and identify by block number)					
<p>The $C_2N_2-O_2$ system has been examined as a source of $N(^2D)$ and $N_2(A^3\Sigma^+)$ with application to an energy transfer chemical laser. Both flowing afterglow and pulsed photodissociation techniques have been used to generate the CN radicals that initiate the chemical generation steps. Laser-induced fluorescence techniques have been used to monitor CN, NCO, and $N_2(A^3\Sigma^+)$. The resonance-enhanced multiphoton ionization (REMPI) technique was developed for $N(^2D)$. During this work, vibrationally excited nitrogen was also characterized by its REMPI signals, and two-photon dissociation of both NO and N_2O were discovered as sources of $N(^2D)$. The REMPI technique was then applied to the $C_2N_2-O_2$ system, in which the presence of $N(^2D)$ was demonstrated and its temporal profile measured. The results to date, in (over)</p>					
20. DISTRIBUTION/AVAILABILITY OF ABSTRACT <input type="checkbox"/> UNCLASSIFIED/UNLIMITED <input checked="" type="checkbox"/> SAME AS RPT. <input type="checkbox"/> DTIC USERS			21. ABSTRACT SECURITY CLASSIFICATION UNCLASSIFIED		
22a. NAME OF RESPONSIBLE INDIVIDUAL Capt Robert P. Crannage, JR.			22b. TELEPHONE (Include Area Code) (505) 844-0731		22c. OFFICE SYMBOL AFWL/ARD

DD Form 1473, JUN 86

Previous editions are obsolete.

SECURITY CLASSIFICATION OF THIS PAGE
UNCLASSIFIED

UNCLASSIFIED

SECURITY CLASSIFICATION OF THIS PAGE

18. SUBJECT TERMS (CONTINUED).

Cyanogen-Oxygen
Laser Induced Fluorescence
Spectroscopy
 $N(^2D)$
 $N_2(A^3\Sigma_u^+)$
CN
NCO
REMPI

19. ABSTRACT (CONTINUED).

conjunction with expectations from computer modeling, suggest that our basic understanding of this system is correct and that the chemistry provides efficient production of both $N(^2D)$ and $N_2(A^3\Sigma_u^+)$.

INS
4

Accession For	
NTIS GRA&I	<input checked="checked" type="checkbox"/>
DTIC TAB	<input type="checkbox"/>
Unannounced	<input type="checkbox"/>
Justification	
By	
Distribution/	
Availability Codes	
Dist	Avail and/or Special
A-1	

CONTENTS

<u>Section</u>	<u>Page</u>
LIST OF FIGURES	iv
CONVERSION TABLE	vi
1.0 BACKGROUND	1
2.0 AFTERGLOW STUDIES	8
3.0 PULSED PHOTODISSOCIATION STUDIES	10
3.1 INTRODUCTION	10
3.2 EXPERIMENTAL METHOD	12
3.3 RESULTS AND DISCUSSION	13
3.3.1 LIF Measurements	13
3.3.2 NO γ -Band Emission	15
4.0 REMPI DETECTION OF N(2D)	27
4.1 INTRODUCTION	27
4.2 EXPERIMENTAL METHOD	28
4.3 RESULTS AND DISCUSSION	30
5.0 KINETIC STUDIES OF N(2D)	34
5.1 INTRODUCTION	34
5.2 EXPERIMENTAL METHOD	35
5.3 RESULTS AND DISCUSSION	35
6.0 REMPI STUDIES IN THE LEWIS-RAYLEIGH AFTERGLOW OF NITROGEN	38
6.1 INTRODUCTION	38
6.2 EXPERIMENTAL METHOD	39
6.3 RESULTS AND DISCUSSION	39
7.0 PHOTOLYTIC SOURCES OF N(2D)	46
7.1 INTRODUCTION	46
7.2 EXPERIMENTAL METHOD	48
7.3 RESULTS AND DISCUSSION	49
8.0 N(2D) MEASUREMENT IN C ₂ N ₂ -O ₂	60
9.0 CONCLUSIONS	63
REFERENCES	64
BIBLIOGRAPHY	72

FIGURES

<u>Figure</u>		<u>Page</u>
1	CN ($v'' = 0$) decay rate versus O_2 concentration.	14
2	Emission spectrum produced by 158-nm radiation of a mixture of C_2N_2 (10^{15} molecules cm^{-3}) and O_2 (10^{15} molecules cm^{-3}) in helium (2.7×10^{17} molecules cm^{-3}).	17
3	Intensity-time profiles of NO γ -band emission for three O_2 concentrations.	20
4	Intensity-time profiles of NO γ -band emission for three NO concentrations.	21
5	Model calculations of time-integrated yields of $N_2(A)$ and NO γ -bands as a function of initial CN concentration.	23
6	Two-photon absorption in $N(^2D)$ and $N(^4S)$ and subsequent ionization and emission processes.	29
7	Three-photon (two to resonance) ionization spectrum from $N(^2D)$.	31
8	Resonance ionization spectrum of N_2 subjected to a microwave discharge versus dye laser wavelength in air (533 to 542 nm).	32
9	I/I_0 versus $[Q]$, for $Q = O_2, C_2N_2$.	36
10	(a) Low-resolution REMPI spectrum, from 254.2 to 262 nm, of a 4:1 N_2/Ar mixture at a total pressure of 7.7×10^{16} molecules cm^{-3} when subjected to a microwave discharge. (b) Effect of replacing the Ar by CO_2 (added after the discharge) in the above experiment.	40

FIGURES (CONCLUDED)

<u>Figure</u>		<u>Page</u>
11	Low-resolution REMPI spectrum, from 244 to 251 nm, of nitrogen at 6.4×10^{16} molecule cm^{-3} subjected to a microwave discharge.	42
12	Power dependences of the ionization signals arising through the excitation of the (12,23), (13,24), and (14,25) LBH transitions in microwave-discharged nitrogen at $\sim 6.4 \times 10^{16}$ molecules cm^{-3} .	43
13	Power dependences of the ionization signals arising through the excitation of the (6,0), (5,0), (3,0), and (2,0) LBH transitions in nitrogen at $\sim 6.4 \times 10^{16}$ molecules cm^{-3} .	44
14	Schematic representation of multiphoton processes.	47
15	QR scan with Q (upper plot) and without Q (lower plot).	50
16	Power dependence of $\text{N}(^2\text{D})$ from N_2 discharge source.	52
17	Power dependence of $\text{N}(^2\text{D})$ from NO photodissociation.	53
18	Ion signal versus [NO], Q and Q/QR scans.	55
19	NO β -band intensity versus $[\text{O}_2]$.	58
20	(a) REMPI signal from $\text{N}(^2\text{D})$ generated in a $\text{C}_2\text{N}_2/\text{O}_2/\text{He}$ mixture 45 μJ after a pulse of 158-nm radiation. (b) Background signal with no O_2 .	61
21	Temporal profile of $\text{N}(^2\text{D})$ generated in a $\text{C}_2\text{N}_2/\text{O}_2/\text{He}$ mixture after a pulse of 158-nm radiation.	62

Conversion factors for U.S. customary
to metric (SI) units of measurement.

To Convert From	To	Multiply By
angstrom	meters (m)	1.000 000 X E -10
atmosphere (normal)	kilo pascal (kPa)	1.013 25 X E +2
bar	kilo pascal (kPa)	1.000 000 X E +2
barn	meter ² (m ²)	1 000 000 X E -28
British thermal unit (thermochemical)	joule (J)	1.054 350 X E +3
cal (thermochemical)/cm ² §	mega joule/m ² (MJ/m ²)	4.184 000 X E -2
calorie (thermochemical)§	joule (J)	4.184 000
calorie (thermochemical)/g§	joule per kilogram (J/kg)*	4.184 000 X E +3
curies	giga becquerel (GBq)+	3.700 000 X E +1
degree Celsius‡	degree kelvin (K)	$t_K = t_C + 273.15$
degree (angle)	radian (rad)	1.745 329 X E -2
degree Fahrenheit	degree kelvin (K)	$t_K = (t_F + 459.67)/1.8$
electron volt§	joule (J)	1.602 19 X E -19
erg§	joule (J)	1.000 000 X E -7
erg/second	watt (W)	1.000 000 X E -7
foot	meter (m)	3.048 000 X E -1
foot-pound-force	joule (J)	1.355 818
gallon (U.S. liquid)	meter ³ (m ³)	3.785 412 X E -3
inch	meter (m)	2.540 000 X E -2
jerk	joule (J)	1.000 000 X E +9
joule/kilogram (J/kg) (radiation dose absorbed)§	gray (Gy)*	1.000 000
kilotons§	terajoules	4.183
kip (1000 lbf)	newton (N)	4.448 222 X E +3
kip/inch ² (ksi)	kilo pascal (kPa)	6.894 757 X E +3
kip	newton-second/m ² (N-s/m ²)	1.000 000 X E +2
micron	meter (m)	1.000 000 X E -6
mil	meter (m)	2.540 000 X E -5
mile (international)	meter (m)	1.609 344 X E +3
ounce	kilogram (kg)	2.834 952 X E -2
pound-force (lbf avoirdupois)	newton (N)	4.448 222
pound-force inch	newton-meter (N·m)	1.129 848 X E -1
pound-force/inch	newton/meter (N/m)	1.751 268 X E +2
pound-force/foot ²	kilo pascal (kPa)	4.788 026 X E -2
pound-force/inch ² (psi)	kilo pascal (kPa)	6.894 757
pound-mass (lbm avoirdupois)	kilogram (kg)	4.535 924 X E -1
pound-mass-foot ² (moment of inertia)	kilogram-meter ² (kg·m ²)	4.214 011 X E -2
pound-mass/foot ³	kilogram-meter ³ (kg/m ³)	1.601 846 X E +1
rad (radiation dose absorbed)§	gray (Gy)*	1.000 000 X E -2
roentgen§	coulomb/kilogram (C/kg)	2.579 760 X E -4
shake	second (s)	1.000 000 X E -8
slug	kilogram (kg)	1.459 390 X E +1
torr (mm Hg, 0° C)	kilo pascal (kPa)	1.333 22 X E -1

*The gray (Gy) is the accepted SI unit equivalent to the energy imparted by ionizing radiation to a mass of energy corresponding to one joule/kilogram.

+The becquerel (Bq) is the SI unit of radioactivity; 1 Bq = 1 event/s.

‡Temperature may be reported in degree Celsius as well as degree kelvin.

§These units should not be converted in DNA technical reports; however, a parenthetical conversion is permitted at the author's discretion.

1.0 BACKGROUND

The most obvious advantage of lasers that derive their major pumping energy from chemical reactions is the compact form in which the energy source can be stored and manipulated. The challenges are to identify the types of chemical reactions that store a significant fraction of the reaction exothermicity in specific modes of excitation, to establish rules to predict and understand this behavior, and to devise schemes for using this stored energy to produce population inversions in species with suitable radiative transitions.

A large number of chemical reactions are known to result in extensive vibrational excitation of the reaction products, primarily in the new bond formed in the reaction. Such processes have led to the development of the most successful and popular HF chemical laser, based on vibrational transitions in HF, whose upper states are produced in the following reaction:



This laser was developed independently by K. L. Kompa and G. C. Pimentel (Ref. 1) and by T. F. Deutch (Ref. 2.). The fundamental processes and their influence on laser performance (Ref. 3) were reviewed by J. J. Hinchey.

For a variety of practical reasons (including atmospheric transmission and diffraction-limited range), there has been considerable interest in chemical lasers that operate at shorter wavelengths. Because the frequencies of the vibrational transitions in HF are about as high as one could find in any molecule, shorter wavelength chemical lasers must necessarily involve electronic transitions. This report is a brief review of the current status of two generic approaches to the development of electronic transition chemical lasers. The first (and so far unsuccessful) approach is to begin by investigating chemical reactions that are known to produce visible light. The second, indirect approach is to choose a reaction known to produce excited states that are not themselves good radiators but can transfer the stored energy to other atoms or molecules.

In many cases, flames involving highly exothermic chemical reactions are observed to produce intense visible emission, referred to as chemiluminescence. It was supposed that this chemiluminescence reflected direct formation of electronically excited molecules in chemical reactions, by a process illustrated schematically as follows:



followed by

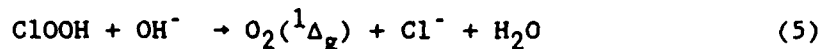
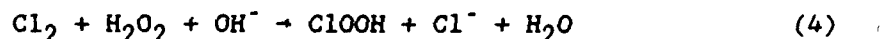


During the past two decades, considerable effort was directed toward identifying and characterizing reactions with high yields of visible emission. A number of high yield reactions were found: for example, $Sm + NF_3$, with a photon yield of 70 percent (Ref. 4). However, in no case was gain or a population inversion observed. Detailed studies (Ref. 4) of the pressure dependence of the photon yields indicated that the chemiluminescence mechanisms are much more complicated than the reactions shown above. All of the observations can be explained by a model that assumes that the initial reaction produces only ground electronic states in high vibrational levels, and that the chemiluminescence results from $V \rightarrow E$ conversion accomplished by collisions with the background gas.

Supporting theoretical studies (Refs. 5 and 6) of the interactions between the electronic potential energy surfaces accessible to the reaction complex led to a reaffirmation of the rule that electronic quantum numbers tend to be conserved in chemical reactions. Thus, while reactions of electronically excited states often have high yields of excited products (e.g., $Kr^* + F_2 \rightarrow KrF^* + F$), ground state reactants can always be expected to yield products in their ground electronic states. Only two types of exceptions are known or expected. The first of these is of only limited use in laser development: if the reaction complex lives long enough, energetically accessible excited states may be populated in a statistical fashion by equipartition of the reaction exothermicity among the vibrational and electronic degrees of freedom. The second type of exception is very important for laser development and is the basis of considerable work now

being performed in various laboratories: selective production of electronically excited states is expected when the ground state reactants, or the only energetically accessible reaction complex, do not have the same spin symmetry as the ground state products. In this case, conservation of electronic quantum numbers (i.e., spin) leads to excited products, provided that the spin-orbit coupling is sufficiently weak. Unfortunately, the products of such spin-conserving reactions are predicted to be radiatively metastable and therefore inconvenient for optical extraction of the stored energy. In such cases, the best way to extract the stored energy may be to transfer energy to another species that is less radiatively metastable.

The only known electronic transition chemical laser, the iodine laser, (Ref. 7) is based on selective chemical production of $O_2(a^1\Delta_g)$ and subsequent energy transfer to atomic iodine. This produces a population inversion on the $I(^2P_{1/2} \rightarrow ^2P_{3/2})$ transition at $1.315 \mu m$, provided that the ratio $[O_2(^1\Delta_g)]/[O_2(^3\Sigma_g^-)]$ is sufficiently large. The reaction of Cl_2 with H_2O_2 in basic solution, although still poorly understood, is known to produce $O_2(a^1\Delta_g)$ in high yield. A plausible reactor sequence is the following:



Reaction (5) is the vital spin-conserving step, in which the only possibility is singlet products, because the only stable state of $ClOOH$ is expected to be a singlet state.

An additional related class of spin-conserving chemical reactions leads to production of the isoelectronic excited $NF(a^1\Delta)$. As for O_2 , the ground state has $^3\Sigma^-$ symmetry. Examples of such reactions include the following (Refs. 8-10):



and

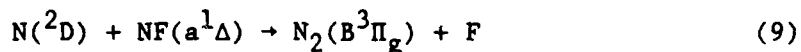


These reactions lead to selective production of excited states because the only stable state of the reaction complex (HNF_2 or FN_3) is a singlet state and the only energetically accessible state of the spectator fragment (HF or N_2) is also a singlet. Also, as for O_2 , the $^1\Delta$ excited state is a poor radiator, and the stored electronic energy must be used either in energy transfer or in subsequent chemical reactions.

An additional disadvantage of both $\text{O}_2(^1\Delta)$ and $\text{NF}(^1\Delta)$ is that their energies are only 1.0 and 1.4 eV, respectively, and thus cannot be the direct energy-transfer precursors of a visible laser. Unlike its oxygen analogue, $\text{NF}(^1\Delta)$ is a relatively reactive species, and its complex chemistry provides additional opportunities for generation of more energetic excited states. The reaction with excess hydrogen atoms (Refs. 8 and 9) is particularly interesting:



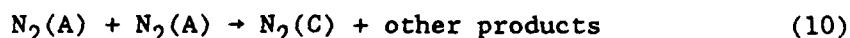
This reaction is also required by spin conservation to yield electronically excited products. The resulting $\text{N}(^2\text{D})$ is also radiatively metastable, but it now contains 2.4 eV of stored electronic energy in addition to its considerable reactivity. These properties are illustrated by the observation of N_2 first-positive emission ($\text{B}^3\Pi_g \rightarrow \text{A}^3\Sigma_u^+$) in $\text{H} + \text{NF}_2$ reaction systems. This results (Refs. 8-11) from the following reaction:



Spin conservation no longer requires that electronically excited products be obtained, but the reaction is very exothermic. Nothing is known about the potential energy surfaces of the N_2F reaction intermediate, but because both reactants start in electronically excited states, the expectation is that conservation of "electronic quantum numbers" would favor electronically excited products. The most recent measurements (Refs. 12 and 13) suggest that this is true.

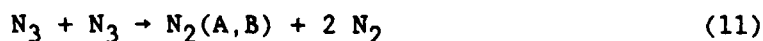
It has been further supposed that if the yield of $\text{N}_2(\text{B}^3\Pi_g)$ is large enough to give a bright emission, the yield of the lower lying, radiatively metastable $\text{N}_2(\text{A}^3\Sigma_u^+)$ state is likely to be even higher. This does not appear

to be true (Ref. 13), and the major source of $N_2(A^3\Sigma_u^+)$ appears to be radiative cascade from $N_2(B^3\Pi_g)$. Transferring the 6.2 eV of electronic energy stored in $N_2(A^3\Sigma_u^+)$ to a suitable laser molecule is an attractive idea. Note, however, that in spite of its long radiative lifetime it is unlikely to be kinetically metastable in any chemical generator operating at a pressure high enough to generate sufficient gain on the target transition. At the very least, the energy pooling reaction



with a rate coefficient (Ref. 13) of $3 \times 10^{-10} \text{ cm}^3 \text{ molecule}^{-1} \text{ s}^{-1}$, is so fast that a density of $10^{16} \text{ molecules cm}^{-3}$ can be supported for only ~300 ns. Reactions of $N_2(A)$ with many species have already been studied experimentally, and most of them are quite fast. This means that the energy transfer acceptor must be present in the gas mixture that is being used to generate the $N_2(A)$, so the choices become more complicated and eventually more limited.

Other sources of $N_2(A)$ have also received attention. These include reactions of the chemically metastable radicals N_3 and the isoelectronic NCO. Schemes to explain the excited nitrogen emissions in azide decomposition tended to emphasize the following radical-radical recombination:



In the most recent work (Ref. 14) on this system, R. D. Coombe found that Reaction (11) was slow ($\sim 3 \times 10^{-12} \text{ cm}^3 \text{ molecule}^{-1} \text{ s}^{-1}$) and that the major source of the emission was the reaction

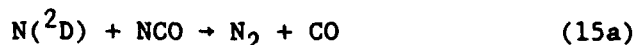


with a rate coefficient of $1.4 \times 10^{-10} \text{ cm}^3 \text{ molecule}^{-1} \text{ s}^{-1}$. Finally, there is the possibility of generating $N_2(A)$ in the oxygen combustion of cyanogen, $(CN)_2$. This system has great potential as a source of electronically excited nitrogen species. Other researchers, N. Basco (Ref. 15) and K. J. Schmatjko and J. Wolfrum (Ref. 16), have demonstrated that two of the principal early reactions in the CN-O₂ afterglow system are as follows:



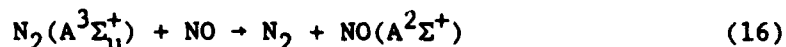
Thus, a copious source of $\text{N}({}^2\text{D})$ is in principle available, to the extent that CN can be efficiently generated. Reactions (13) and (14) are both fast, with rate coefficients of $7.6 \times 10^{-12} \text{ cm}^3 \text{ molecule}^{-1} \text{ s}^{-1}$ and $1.7 \times 10^{-11} \text{ cm}^3 \text{ molecule}^{-1} \text{ s}^{-1}$, respectively. More recent work (Refs. 17 and 18) on Reaction (13) shows it to be even faster: values of $(2.0 \pm 0.2) \times 10^{-11} \text{ cm}^3 \text{ molecule}^{-1} \text{ s}^{-1}$ and $(2.5 \pm 0.2) \times 10^{-11} \text{ cm}^3 \text{ molecule}^{-1} \text{ s}^{-1}$ were obtained for the $v = 0$ level of CN and a value of $(2.4 \pm 0.1) \times 10^{-11} \text{ cm}^3 \text{ molecule}^{-1} \text{ s}^{-1}$ was obtained for the $v = 1$ level.

As a consequence of these two reactions proceeding rapidly and with high yields, the production rates of both NCO and $\text{N}({}^2\text{D})$ are high. These high production rates raise the interesting possibility that these species could interact as follows:



Reaction (15a) is enormously exothermic, ΔH being 233 kcal/mol ($> 10 \text{ eV}$), so that even production of such energetic species as $\text{N}_2(\text{A}^3\Sigma_u^+)$ and $\text{CO}(\text{a}^3\Pi)$ is easily accommodated. In fact, all N_2 states up to the dissociation limit are accessible. This research was designed to determine whether Reaction (15a) is the dominant one and if its products are excited.

Previous experiments had confirmed that NCO is produced in the CN- O_2 system, and emissions from energetic species had been seen, specifically the 8-eV $\text{CO}(\text{A}^1\Pi)$ state and the 6-eV $\text{NO}(\text{A}^2\Sigma^+)$ state. The latter state is often indicative of the presence of $\text{N}_2(\text{A}^3\Sigma_u^+)$, because of the following energy transfer reaction:



However, it was not known if these products were a result of Reaction (15a).

Because the CN-O system is known to produce $N(^2D)$ and may lead to production of electronically excited N_2 , the options exist for using $N(^2D)$ in some other reaction sequence [there may be some advantage in generating $N(^2D)$ by Reaction (14) rather than Reaction (8)] and for investigating the $N(^2D)$ -NCO system to determine whether the great exothermicity of Reaction (15a) is in fact useful.

In these experimental studies of the CN- O_2 system, two different approaches were used for generating CN radicals and studying the subsequent chemistry. The early work involved the flowing afterglow technique and the later experiments used pulsed photodissociation. Laser induced fluorescence (LIF) was used to probe CN, NCO, and $N_2(A^3\Sigma_u^+)$ directly in these studies, and monitor of $N_2(A^3\Sigma_u^+)$. SRI International also developed the resonance-enhanced multiphoton ionization (REMPI) technique to detect $N(^2D)$, to measure $N(^2D)$ kinetics, and to determine $N(^2D)$ concentrations and time evolutions in the $C_2N_2-O_2$ mixture. The results of these studies and the REMPI signals from vibrationally excited N_2 and the photolytic sources of $N(^2D)$ discovered in the course of this work are discussed in the following sections.

2.0 AFTERGLOW STUDIES

For these studies, CN radicals were generated in two ways. In one, C_2N_2 was added to flowing afterglows in N_2 or He. In another, HCN was used as the CN radical source (the H was abstracted with the F atoms from a microwave discharge in a dilute mixture of CF_4 in helium or argon). The CN stream was then split in two. In one section, the CN/ O_2 reaction, Reaction (13), was used to generate NCO. In the other section, the addition of oxygen atoms (by titrating N atoms from a N_2 discharge with NO) was used to generate $N(^2D)$ by Reaction (14). When the flows in the two sections were combined, Reaction (15) could occur.

Much of the complicated secondary chemistry introduced with C_2N_2 as the CN source was not present when HCN was used as the CN source. For example, with the latter CN source, oxygen and nitrogen atoms both cause rapid removal of CN and NCO. This behavior was anticipated for CN from the known fast rate coefficients for Reaction (14) and the following reaction:



$[k_{17} = (1.0 \pm 0.13) \times 10^{-10} \text{ cm}^3 \text{ molecule}^{-1} \text{ s}^{-1}]$ (Ref. 19). The rate coefficients for NCO reactions with oxygen and nitrogen atoms have not been determined, but fast rates are anticipated (Ref. 20). This behavior contrasts with the enhancements observed in the CN + N and O and NCO + O systems observed in the presence of C_2N_2 .

Using known sources of $N_2(A^3\Sigma_u^+)$, it was established that the detection sensitivity of the LIF technique was $\sim 5 \times 10^9 \text{ molecules cm}^{-3}$, while γ -band emission produced by Reaction (16) when optimum NO is added provides ~ 50 times more sensitivity. In spite of this high sensitivity for $N_2(A)$, this species could not be detected in the CN/ O_2 /O system with initial CN densities $\geq 10^{12} \text{ molecules cm}^{-3}$ and Ar as the buffer gas. The fast wall losses in the system, measured for CN, NCO, and $N_2(A)$ and presumably applying to $N(^2D)$ as well, prevented any simple interpretation of why $N_2(A)$ was not observed. Some simple computer modeling showed that even if Reaction (15) had a rate

coefficient of $10^{-10} \text{ cm}^3 \text{ molecule}^{-1} \text{ s}^{-1}$ and a 100 percent yield of $\text{N}_2(\text{A})$, the predicted $\text{N}_2(\text{A})$ densities in the observation bulb would be only in the 10^8 - 10^9 molecules cm^{-3} range for an initial CN concentration of $\sim 10^{12}$ molecules cm^{-3} .

An attempt was made to minimize the dominant role of the wall losses by replacing the argon buffer gas with helium. This increased the flow velocity, and $\text{N}_2(\text{A})$ could be detected even with the LIF technique. However, in this system, NCO was not involved in $\text{N}_2(\text{A})$ generation, because the O_2 needed for NCO generation by Reaction (13) could be turned off. The necessity of adding some oxygen atoms suggested that the $\text{N}(^2\text{D})$ produced by Reaction (14) was a necessary reactant. Because complete titration of the N atoms removed the $\text{N}_2(\text{A})$ signal, it appeared that the products of a microwave discharge in CF_4 (or CF_4/He) must be allowed to interact with active nitrogen. In addition to producing CN, the resulting chemistry is also likely to produce NF species. The reaction



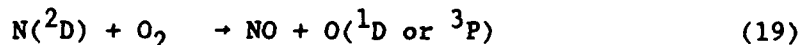
may have produced the $\text{N}_2(\text{A})$ observed. This reaction can be compared with Reaction (9), in which $\text{N}_2(\text{B}^3\Pi_g)$ is produced when $\text{NF}(\text{a}^1\Delta)$ reacts with $\text{N}(^2\text{D})$. In the SRI system, the absence of strong $\text{N}_2(\text{B})$ 1+ emission or any evidence for electronically excited states of NF (the $\text{a}^1\Delta$ emits at 874 nm and the $\text{b}^1\Sigma$ emits at 529 nm) suggested that Reaction (9) followed by $\text{N}_2(\text{B} \rightarrow \text{A})$ emission was not the source of the $\text{N}_2(\text{A})$ observed.

Attempts to reduce the wall losses by coating the walls of the flow system with Teflon were not successful, and this approach was therefore judged to be less promising for studying reaction mechanisms than the alternative technique of pulsed photodissociation.

3.0 PULSED PHOTODISSOCIATION STUDIES

3.1 INTRODUCTION

In the cyanogen-oxygen system, a number of chemical pathways can produce NO. For example, in addition to the 6 percent yield from Reaction (13), NO will also be generated by



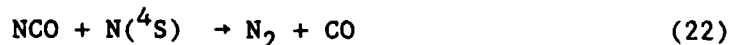
and



In the presence of any NO, any $\text{N}_2(\text{A})$ will manifest itself by Reaction (16), a very efficient energy transfer process, with subsequent emission of the NO γ -bands. This emission has been reported before (Ref. 21 and 22) and attributed to energy transfer from $\text{N}_2(\text{A})$ or CO ($\text{a}^3\Pi$) formed by



or



Although information has been obtained on all the chemiluminescence features of the CN- O_2 system, the focus of this study was on the NO γ -bands and the contributions of the various reactions that might produce them.

In contrast to previous studies, which used steady state measurements in afterglows, this work employed photodissociation of C_2N_2 to generate CN radicals and initiate the chemistry. The initial measurements used the F_2 (158 nm) emission from an excimer laser. In addition to dissociating C_2N_2 ($\sigma = 1.6 \times 10^{-17} \text{ cm}^2$), this also generates atomic oxygen by O_2 photodissociation ($\sigma = 8 \times 10^{-18} \text{ cm}^2$).

Photodissociation of C_2N_2 and O_2 with 158-nm radiation generates the CN radicals and O atoms in the same cell, so that the wall loss problem associated with the flowing afterglow approach is much less important. Furthermore, the strong absorption cross sections of C_2N_2 and O_2 at 158 nm

allow much higher radical and atom densities to be generated, and these higher densities further minimize the effects of wall loss.

After CN and O were produced by photolysis, LIF was used to monitor the disappearance of CN and the appearance and disappearance of NCO. The disappearance of CN and the appearance of NCO were explained by the known kinetics for Reaction (13). The disappearance of NCO was a function of the laser flux and was clearly controlled by a reaction intermediate. This observation did not prove that Reaction (15) constituted an important loss of NCO, because other radical/atom removal processes for NCO could be important. For example, the reaction of NCO with oxygen atoms, Reaction (20), is also expected to be fast.

In addition to these LIF studies, emissions from CN(B) in $v' = 0$ and 1, CN(A) up to $v' = 14$, NO(A), and the triatomic emitters NCN(A), CCN(A), and NCO(A) were also observed. These same emissions were also seen when 193-nm (ArF) radiation was used to dissociate the C_2N_2 ($\sigma \sim 10^{-19} \text{ cm}^2$; Ref. 23). In the latter case, the oxygen atoms in the system were produced by Reaction (13) and not by O_2 photodissociation. Radiation at 193 nm was also used to measure the temporal profiles of the NO γ -bands for various O_2 pressures and also for several NO pressures at fixed O_2 (and C_2N_2) pressure.

The observation of the γ -bands of NO suggested the presence of $N_2(A)$ and the production of NO(A) by Reaction (16). Evidence to support this view was obtained when adding a small amount of NO to the system resulted in enhanced γ -band emission and an increase in its decay rate. These results would be expected for $N_2(A)$ removal by Reaction (16), which has a rate coefficient of $7 \times 10^{-11} \text{ cm}^3 \text{ molecule}^{-1} \text{ s}^{-1}$, in competition with the following reaction:



which has a rate coefficient (Ref. 24) of $5.6 \times 10^{-11} \text{ cm}^3 \text{ molecule}^{-1} \text{ s}^{-1}$.

Further support for Reaction (15) as the source of $N_2(A)$ was provided by studies (Ref. 25) of the very similar reaction of $N(^4S)$ with the isoelectronic N_3 . These studies indicated at least a 20 percent yield of $N_2(B^3\Pi_g)$, which then produces $N_2(A)$ by $1+$ radiation. However, the most convincing evidence for the importance of Reaction (15) as the source of $N_2(A)$ came from measurements of the absolute yield of γ -bands and from measurements of their

temporal profile and comparisons with predictions from a computer model of the chemistry in this system.

3.2 EXPERIMENTAL METHOD

Most of the apparatus has been described in Ref. 26. In most cases, the intensity of the excimer photolysis beam in the center of the photolysis cell was increased by using a MgF_2 lens (focal lengths from 25 cm to 1 m were used). Typical energies transmitted through the cell were 0.5-2 mJ of 158 nm radiation and 10-80 mJ of 193-nm radiation.

For the LIF studies, a Quanta-Ray* Nd: YAG dye laser system provided 5-10 mJ in the region of the (0,0) CN(B-X) transition at 388 nm (using Exciton LD 390). This same dye solution was also used to monitor NCO, pumping the $\text{A}^2\Sigma^+(001) - \text{X}^2\Pi_1(000)$ transition at 398 nm and detecting the $\text{A}^2\Sigma^+(001) - \text{X}^2\Pi_1(001)$ emission at 431 nm. For some of the NCO measurements the dye solution was changed, and the $\text{A}^2\Sigma^+(000) - \text{X}^2\Pi_1(000)$ transition at 440 nm was used for both excitation and observation. The lasers were operated at 10 Hz and were adjusted to overlap spatially along the length of the photolysis cell. For determining the kinetics of the CN and NCO radicals, a variable delay could be introduced between the two laser pulses. Baffles with 1-cm diameter holes were situated in the side arms of the cell to reduce scattered light. The cell was also equipped with MKS Baratron** pressure gauges and was evacuated with a small rotary pump that gave ≈ 20 s for the residence time of the gas in the cell. Some measurements were also made with the residence time reduced to ≈ 2 s to confirm that the results were not affected by any accumulation of photolysis products.

The detection system, situated perpendicular to the laser beams, consisted of a 0.25-m monochromator equipped with an RCA*** C31034 photo-multiplier. Its output passed to a boxcar averager and then to a chart recorder. The gases used were supplied by Matheson**** Gas Products and were

* Manufactured by Quanta-Ray Division of Spectra Physics, 1250 W. Middlefield Rd. P.O. Box 7013, Mountain View, CA 94039.

** Manufactured by MKS Instruments, Inc. Six Shattuck Rd., Andover, MA 01810.

*** Manufactured by RCA Electronic Components, Harrison, NJ 07029.

**** Matheson Gas Products, 6775 Central Avenue, Newark, CA. 94560

used without further purification. The gases passed through flow meters and mixed before entering the photolysis cell.

For measuring the temporal profiles of the chemiluminescent emissions, the boxcar was replaced with an MCA* (ND 100) interfaced to a DEC** VAX 11/750, which was used for data storage and analysis. Most of the NO γ -band measurements were made with the monochromator on the strongest γ -band, the (0,1) band at 237 nm.

3.3 RESULTS AND DISCUSSION

3.3.1 LIF Measurements

The most recent measurements (Refs. 17 and 18) of the rate coefficient for Reaction (13) give values a factor 2 to 3 times higher than those in a number of earlier studies. To determine if the occurrence of Reaction (14), or other complicating chemistry [e.g., $\text{CN} + \text{N}(^4\text{S} \text{ or } ^2\text{D}) \rightarrow \text{C} + \text{N}_2$] might be contributing to the higher recent values, the decay rate of the CN radicals was measured for both high and low concentrations of added O_2 . The measurements at low O_2 are shown in Fig. 1. The slope of the line gives a rate coefficient, k_1 , of $2.0 \times 10^{-11} \text{ cm}^3 \text{ molecules}^{-1} \text{ s}^{-1}$ for Reaction (13), for $v'' = 0$, and was, within experimental error, the same value obtained at larger O_2 additions (up to $2.6 \times 10^{15} \text{ molecules cm}^{-3}$) and in Refs. 17 and 18. At the low O_2 additions, because the CN concentrations produced by photodissociation were comparable to the O_2 addition, the good single-exponential decays of CN provide further evidence that the values of k_1 and k_2 are very similar, because the depletion of O_2 and its replacement by O did not lead to a significant change in the observed decay. A few measurements of CN removal by NO confirmed that the reaction was slow, as expected from the recent measurement of $(1.6 \pm 0.3) \times 10^{-13} \text{ cm}^3 \text{ molecule}^{-1} \text{ s}^{-1}$ for $v'' = 0$ (Ref. 27). It appears that, despite the extensive chemiluminescent phenomena, the behavior of CN radicals is explained by Reactions (13) and (14).

* Multichannel analyzer manufactured by Nuclear Data, Inc., Golf and Meacham Roads, Schaumburg, IL 60172.

** Manufactured by Digital Equipment Corporation, Maynard, MA.

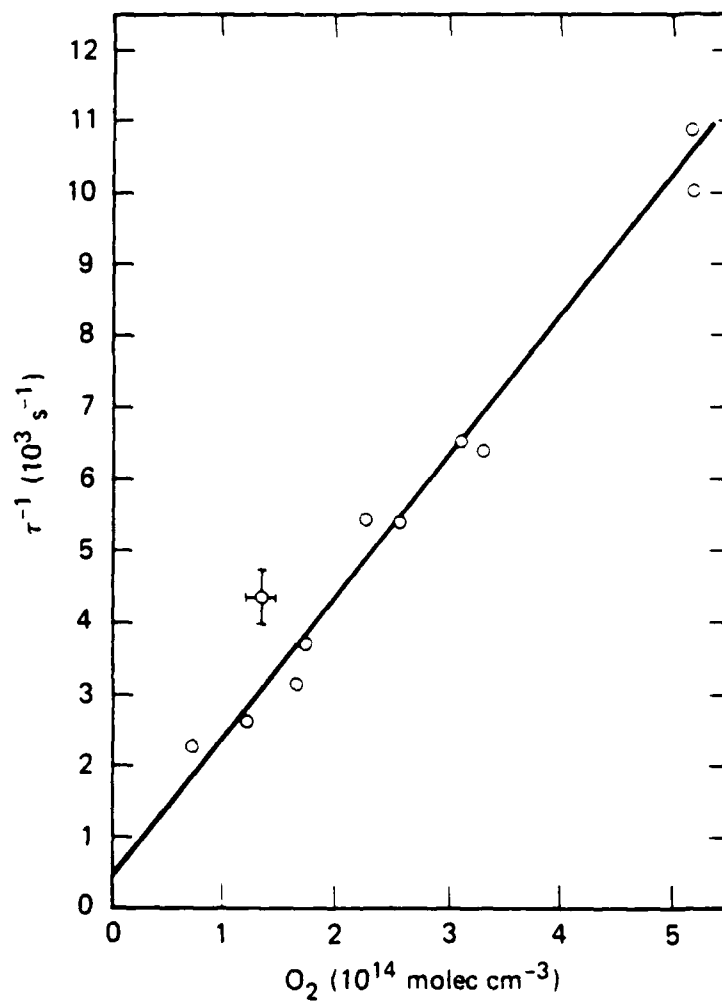


Figure 1. $\text{CN}(v'' = 0)$ decay rate versus O_2 concentration.
 C_2N_2 (10^{15} molecules cm^{-3}) in Ar (3.2×10^{17} molecules cm^{-3}). F_2 laser (158 nm) photodissociation.

The behavior of the NCO was much more complicated. In this case the decay of NCO was not controlled by either C_2N_2 or O_2 . With NO addition, the fast ($k = 3.3 \times 10^{-11} \text{ cm}^3 \text{ molecule}^{-1} \text{ s}^{-1}$; Refs. 28 and 29) removal reaction



was seen and would decrease the NCO lifetime to that of the CN precursor. However, in the absence of NO, the decay of NCO was found to be determined by the excimer intensity, and the decay rate appeared to be roughly proportional to the initial NCO signal. Because the decay was exponential, removal by an $NCO + NCO$ reaction cannot be dominant. What seems most likely is that removal of NCO by reaction with O [Reaction (20)] is an important loss mechanism. This reaction has been postulated in a number of earlier studies (Refs. 15, 30, and 31) and should be fast. The modeling studies (see pg. 18), using the kinetic scheme shown in Table 1, confirmed that the major loss of NCO would be by reaction with O under a variety of conditions [although this depends on an estimated rate coefficient of $1.7 \times 10^{-11} \text{ cm}^3 \text{ molecule}^{-1} \text{ s}^{-1}$ for Reaction (20)]. It can be seen that Reaction (20) produces NO, so that, if Reactions (24) and (20) have similar rate coefficients, the observed single-exponential decay may be explained. It was clear, however, that this study could not give a good value of the rate coefficient for Reaction (20) or assess the role of other NCO removal processes [like Reaction (15)], so further attempts to characterize NCO chemistry by LIF measurements in this system were abandoned.

3.3.2 NO γ -Band Emission

Figure 2 shows the emission spectrum produced by 158-nm radiation of a C_2N_2 - O_2 mixture. The strongest chemiluminescent features are the CN(A) and CN(B) emissions [CN(A) up to $v' = 5$ can be made directly at 158 nm]. A very similar spectrum was obtained with 193-nm radiation [in this case CN(A) cannot be made directly, and the LIF studies revealed CN(X) produced in only the $v'' = 0$ and 1 levels]. In addition, emissions at 466, 440, and 329 nm are thought to arise from the triatomic radicals CCN, NCO, and NCN, respectively. Between 200 and 300 nm lies the weakest chemiluminescent feature, the NO γ -bands. The CO 4+ emission from $CO(A^1\Pi)$ has also been measured between 130 and 180 nm, but its intensity relative to the other features is not shown in Fig. 2. This NO γ -band emission is mainly from $v' = 0$,

Table 1. Reaction Scheme for $N_2(A)$ generation and NO γ -band emission in photodissociated C_2N_2/O_2 mixtures

Reaction Number ^a	Reaction	ΔH (298K) (kcal/mol)	Rate Coefficient ($cm^3 molecule^{-1} s^{-1}$)	Source
	CN \rightarrow wall		900 ^b	Measured
13	CN + O ₂ \rightarrow NCO + O	-7	2.2×10^{-11}	17,18
14	CN + O \rightarrow N(² D) + CO	-22	1.4×10^{-11}	16
	CN + N \rightarrow N ₂ + C	-46	1.0×10^{-10}	32
21	CN + NO \rightarrow N ₂ + CO	-152 ^c	1.4×10^{-13}	27,33
	NCO \rightarrow wall		900 ^b	Estimate
20	NCO + O \rightarrow NO + CO	-101	1.7×10^{-11}	34
22	NCO + N \rightarrow N ₂ + CO	-176 ^c	3.3×10^{-11}	34
15a	NCO + N(² D) \rightarrow N ₂ (A) + CO	-89 ^c	1.0×10^{-10}	Estimate
24	NCO + NO \rightarrow N ₂ O + CO	-65	3.3×10^{-11}	28,29
	NCO + C \rightarrow CN + CO	-130	3.3×10^{-11}	Estimate
	N(² D) \rightarrow wall		900 ^b	Estimate
19	N(² D) + O ₂ \rightarrow NO + O	-86	7.0×10^{-12}	35
	N(² D) + O \rightarrow N + O	-55	1.8×10^{-12}	36
	N(² D) + N ₂ \rightarrow N + N ₂	-55	1.7×10^{-14}	37
	N(² D) + CO \rightarrow N + CO	-55	2.5×10^{-12}	37
	N(² D) + NO \rightarrow N ₂ + O	-130	6.3×10^{-11}	37
	N(² D) + CN \rightarrow N ₂ + C	-101	1.0×10^{-10}	Estimate
	N ₂ (A) \rightarrow wall		900 ^b	Estimate
	N ₂ (A) + O ₂ \rightarrow N ₂ + O + O	-22	3.0×10^{-12}	38,39
	N ₂ (A) + O \rightarrow N ₂ + O	-142	3.0×10^{-11}	40
16	N ₂ (A) + NO \rightarrow N ₂ + NO(A) \rightarrow γ -bands	-142	8.0×10^{-11}	41
25	N ₂ (A) + N ₂ (A) \rightarrow N ₂ + N ₂ (A)	-142	3.0×10^{-10}	41,42
	N ₂ (A) + CO \rightarrow N ₂ + CO	-142	4.0×10^{-12}	43,44
	N ₂ (A) + N \rightarrow N ₂ + N	-142	5.0×10^{-14}	45
	C + NO \rightarrow CN + O	-29	1.1×10^{-10}	46
	C + O ₂ \rightarrow CO + O	-137	3.3×10^{-11}	46
	N + NO \rightarrow N ₂ + O	-75	2.7×10^{-11}	47
13	CN + O ₂ \rightarrow CO + NO	-108	1.4×10^{-12}	16
14	CN + O \rightarrow N + CO	-77	3.0×10^{-12}	16
	C + C ₂ N ₂ \rightarrow C ₂ N + CN	-8	3.0×10^{-11}	32
26	N(² D) + C ₂ N ₂ \rightarrow C ₂ N + N ₂	-109	7.0×10^{-11}	Estimate
23	N ₂ (A) + C ₂ N ₂ \rightarrow N ₂ + CN + CN	-8	4.0×10^{-11}	43
	C ₂ N + N \rightarrow CN + CN	-38	2.0×10^{-11}	Estimate
27	C ₂ N + O \rightarrow CO + CN	-115	2.0×10^{-11}	Estimate
	O \rightarrow wall		900 ^b	Estimate
	N \rightarrow wall		900 ^b	Estimate
	C ₂ N \rightarrow wall		900 ^b	Estimate
	C \rightarrow wall		900 ^b	Estimate

a Numbers are Reference citations.

b In units of s⁻¹

c Reactions with sufficient exothermicity to produce N₂(A).

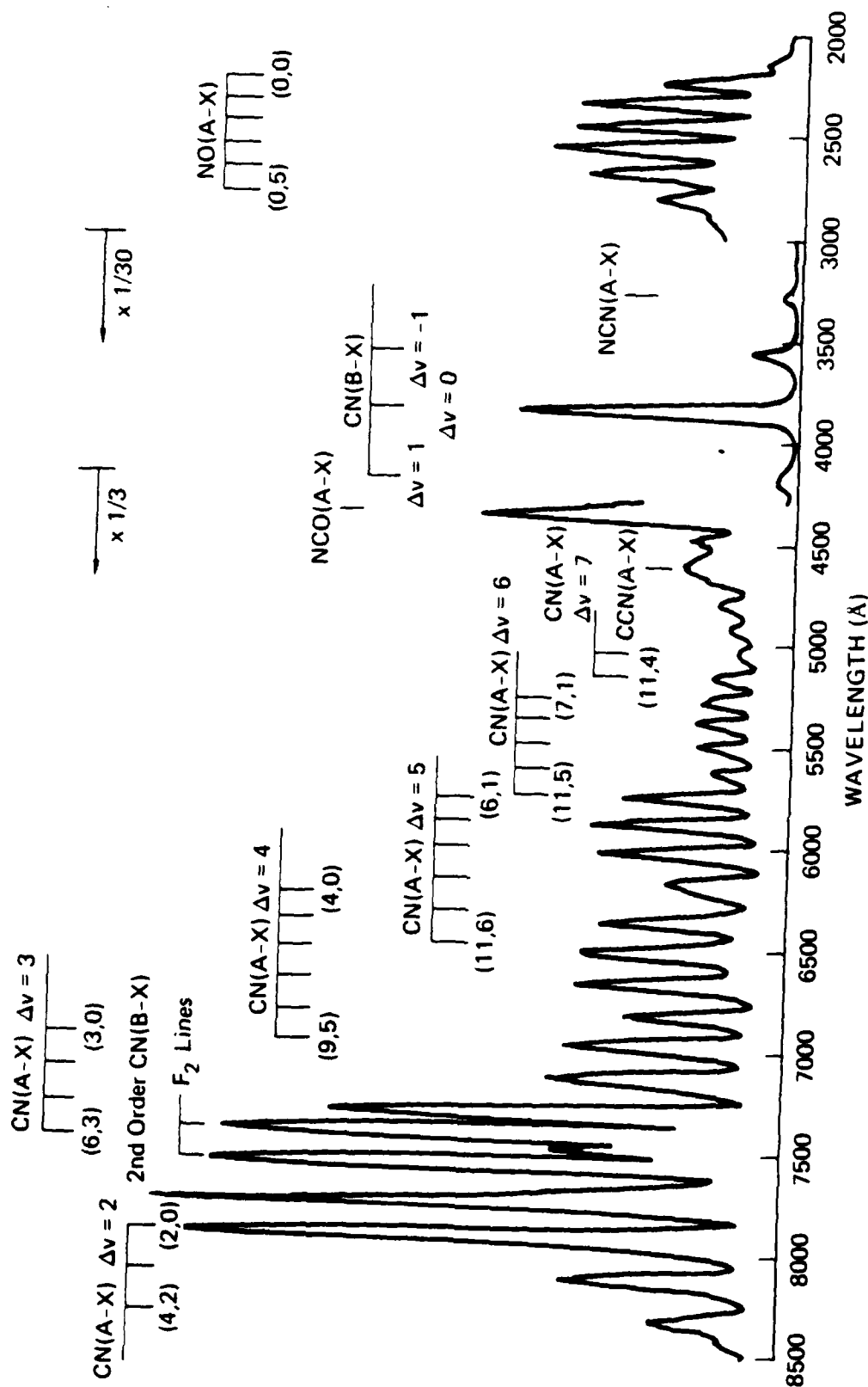


Figure 2. Emission spectrum produced by 158-nm radiation of a mixture of C_2N_2 (10^{15} molecules cm^{-3}) and O_2 (10^{15} molecules cm^{-3}) in helium (2.7×10^{17} molecules cm^{-3}). NO γ -band emission region (2000–3000 Å) enhanced by addition of NO (9×10^{14} molecules cm^{-3}). Spectrum uncorrected for spectral response.

which must closely represent initial production, because vibrational relaxation of NO(A) is small under the experimental conditions. The visible (1,0) band at 215 nm, when corrected for spectral response, indicates that ≥ 80 percent of the emission comes from $v' = 0$. A small (millitorr)* addition of NO enhances the emission without changing its spectral distribution. The spectral distribution of the emission is strong evidence that the species transferring its energy to NO is $N_2(A^3\Sigma_u^+)$, which is known (Ref. 43) to produce >80 percent of the NO($A^2\Sigma^+$) in $v' = 0$. The barely discernible feature on the long wavelength shoulder of the (0,5) γ -band (but more apparent in other spectra) may be the (0,6) NO β -band, which would indicate a small contribution by energy transfer from CO($a^3\Pi$) (Ref. 48), which could also be produced by Reaction (15a). This is in contrast to the substantial yield of NO($B^2\Pi_r$) in thermal collisions (Ref. 48) of CO($a^3\Pi$) with NO. More recent work (Ref. 49) at higher energies, under single-collision conditions in a beam, shows that the energy transfer favors NO($A^2\Sigma^+$) production and discusses this difference. Temporal profiles of the γ -band emission (using 193-nm photolysis) were recorded in cyanogen-oxygen and cyanogen-oxygen-nitric oxide mixtures.

Of the three reactions sufficiently exothermic to produce $N_2(A)$ [Reactions (15a), (21), and (22)], Reaction (22) can be dismissed in the cyanogen-oxygen system because it is slow and because the NO γ -band yield is enhanced by O_2 addition to a cyanogen-NO mixture rather than suppressed, as it would be if Reaction (21) were the $N_2(A)$ source.

Because the NCO kinetics observed in the LIF studies were not understood and because $N(^2D)$ and $N(^4S)$ were not measured, it was decided to proceed with a computer model of the chemistry to attempt to determine the roles of Reactions (15a) and (22) in generating $N_2(A)$ and producing the measured temporal profiles of NO γ -band emission.

* 1 torr = 1.3332×10^2 nm⁻² (or pascal).

The computer simulation was carried out with the aid of the OLCHEM Chemical Kinetics program developed by G. Z. Whitten (now of Systems Applications Incorporated*) and adapted by A. Baldwin (now at Intel Corporation**) and D. M. Golden, (of SRI's Chemistry Laboratory***). Table 1 shows the total reaction scheme. When possible, measured rate coefficients were used, but a number of rate coefficients were estimated [for example, for the important $N(^2D) + CN$ reaction, the measured rate (Ref. 32) for $N(^4S) + CN$ was used]. For some reactions, previous estimates of rate coefficients were used. Estimates from Ref. 33 were used, for example, for the reactions $NCO + O$ and $NCO + N$. Diffusive losses play an important part. The temporal profile experiments used He (10 torr) as the buffer gas. The measured CN diffusive loss rate with this buffer gas was $\approx 900 \text{ s}^{-1}$ [as compared with $\approx 450 \text{ s}^{-1}$, when 10-torr Ar was used as the buffer gas. See Fig. 1]. Because there were no measurements, the same diffusive loss rate was used for all the transient species. Much of the chemistry shown in Table 1 plays a very minor role: it was included to suggest ways of making the CN(A and B) and triatomic chemiluminescent emissions that may be the subject of future study. The temporal behavior of the CO 4+ emission (Ref. 50), particularly its variation with oxygen concentration, was very similar to that of the NO γ -bands. Reaction (15a) can produce either CO 4+ emission or $N_2(A)$, and the similar temporal behaviors provide good evidence for Reaction (15a) as the important reaction. Reaction (22) is not sufficiently exothermic to produce CO 4+.

Figure 3 shows experimental γ -band profiles for three O_2 concentrations and the computed profiles with either Reaction (15a) or Reaction (22) as the $N_2(A)$ source. Clearly, Reaction (15a) provides the better fit. Variation of the temporal profiles as a function of added NO is similar for the two reactions, as Fig. 4 shows.

Further evidence to support Reaction (15a) as the dominant reaction was found in measurements of the absolute γ -band yield. For these measurements, the F_2 laser was used on a mixture of C_2N_2 and O_2 ($10^{15} \text{ molecules cm}^{-3}$) in He ($2.7 \times 10^{17} \text{ molecules cm}^{-3}$) and the intensity of the CN(A \rightarrow X) (2,0) band was

* Systems Applications Inc., 101 Lucas Valley Road, San Rafael, CA 94903.

** Intel Corporation, 2050 Mission College Blvd., Santa Clara, CA 95052.

*** Chemistry Laboratory, SRI International, 333 Ravenswood Avenue, Menlo Park, CA 94025

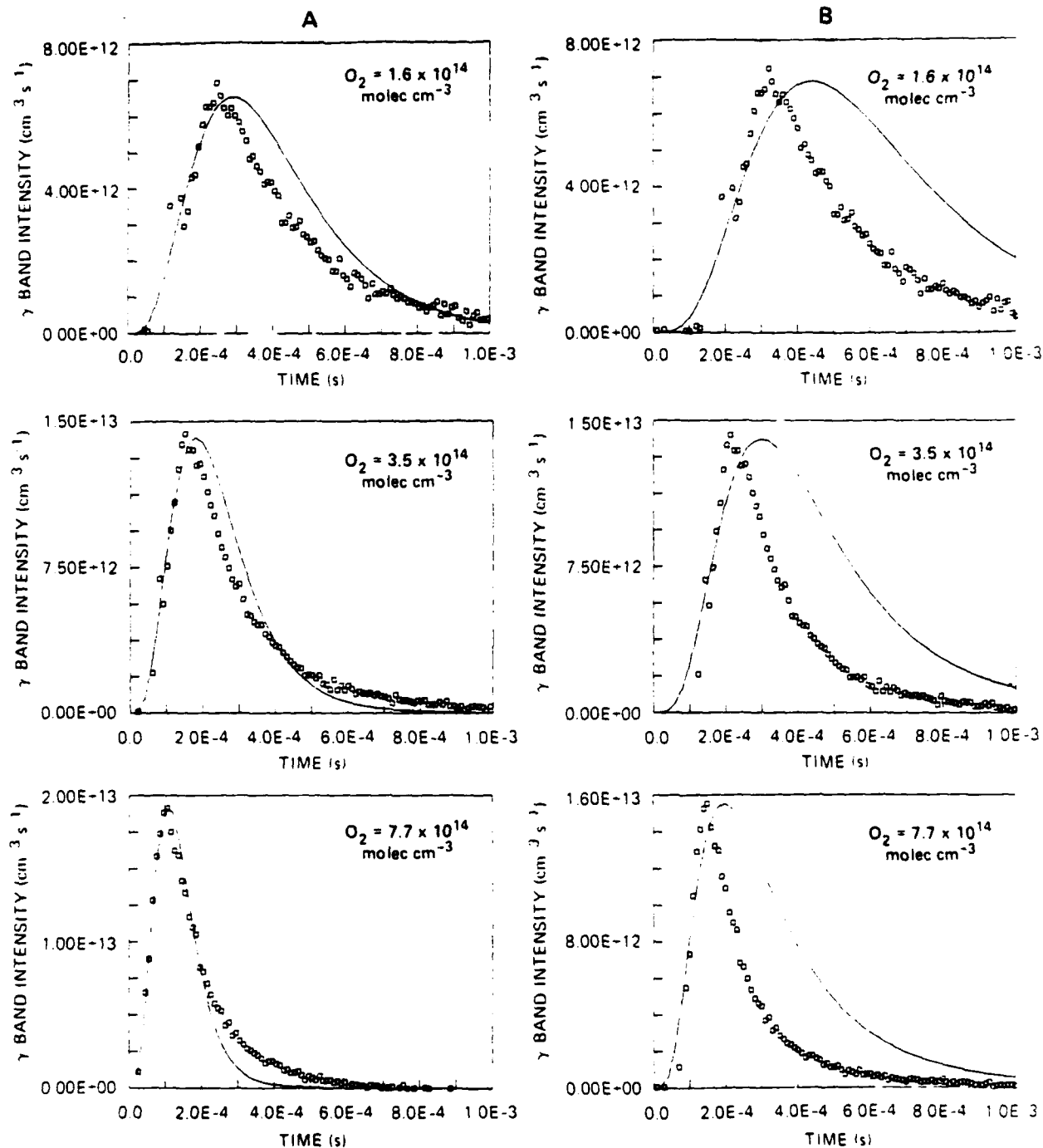


Figure 3. Intensity-time profiles of NO γ -band emission for three O_2 concentrations: ----, model; \square , normalized experimental points.

Experimental conditions were $[He] = 3.5 \times 10^{17}$ molecules cm^{-3} , $[C_2N_2] = 10^{15}$ molecules cm^{-3} , and O_2 concentrations as shown. In addition to these inputs, model calculations used initial $[CN] = 10^{14}$ molecules cm^{-3} . A = $N(2D) + NCO$ as only $N_2(A)$ source; B = $N(4S) + NCO$ as only $N_2(A)$ source.

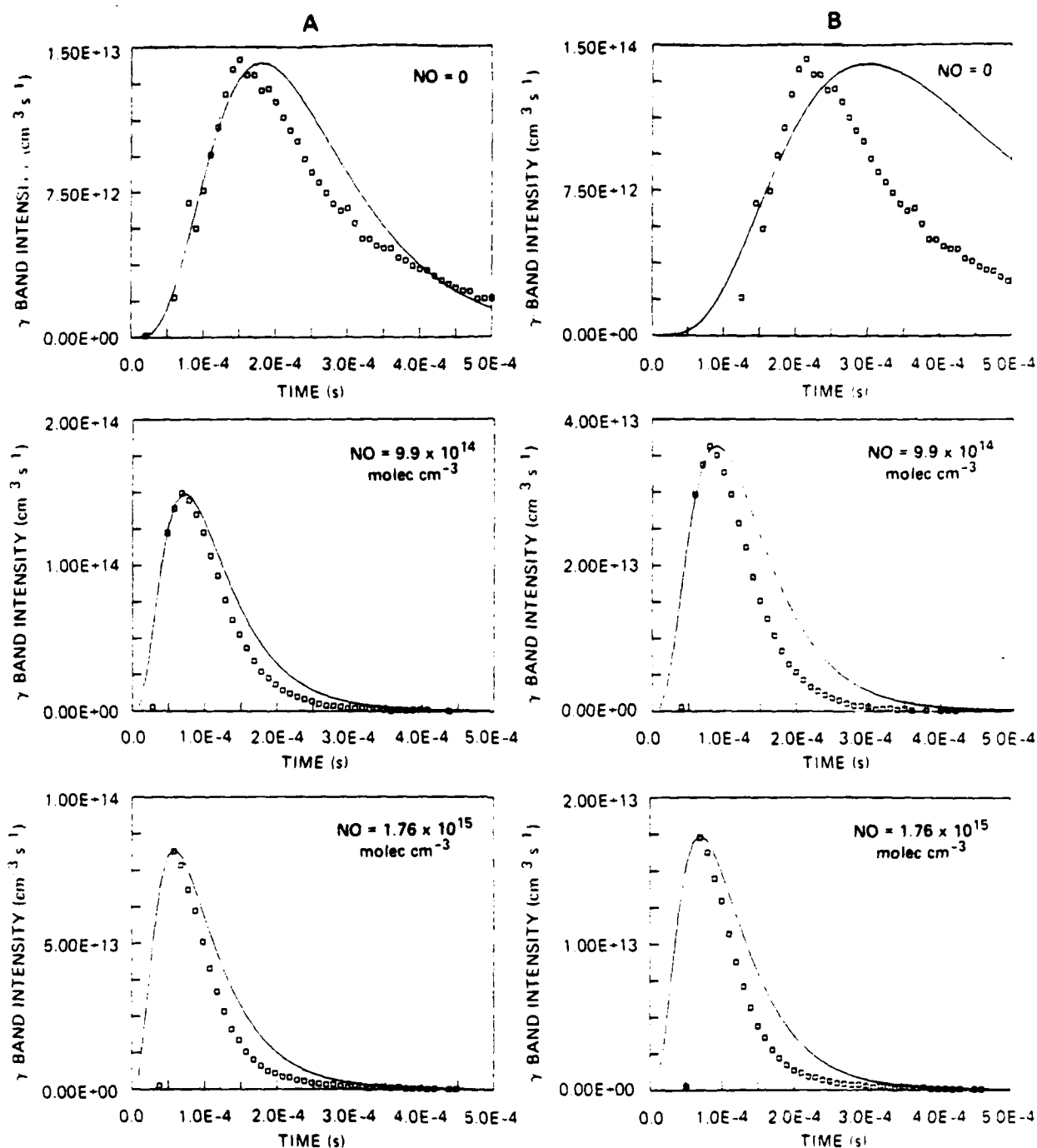


Figure 4. Intensity-time profiles of NO γ -band emission for three NO concentrations: —, model; \square , normalized experimental points.

Experimental conditions were $[\text{He}] = 3.5 \times 10^{17}$ molecules cm^{-3} , $[\text{C}_2\text{N}_2] = 10^{15}$ molecules cm^{-3} , $[\text{O}_2] = 3.6 \times 10^{14}$ molecules cm^{-3} , and NO concentrations as shown. In addition to these inputs, model calculations used initial $[\text{CN}] = 10^{14}$ molecules cm^{-3} . A = $\text{N}(^2\text{D}) + \text{NCO}$ as only $\text{N}_2(\text{A})$ source; B = $\text{N}(^4\text{S}) + \text{NCO}$ as only $\text{N}_2(\text{A})$ source.

used as an internal actinometer. Previous work in this laboratory (Ref. 51) had established a $\text{CN(A)}_{v'=2}$ quantum yield of ≈ 50 percent at 158 nm. The monochromator-photomultiplier combination was calibrated with standard lamps, and the sensitivity at the (0,1) NO γ -band at 237 nm was found to be a factor of 2.2 larger than the sensitivity at the $\text{CN(A-X)} (2,0)$ band at 787 nm. The $\text{CN(A)}_{v'=2}$ emission intensity was found to be linear in laser energy, and its intensity was not enhanced by O_2 addition, so that any chemiluminescence was small compared to the direct production. Based on spectroscopic information on Franck-Condon factors and transition moments, the (0,1) γ -band corresponds to ≈ 30 percent of the γ -band emission from $v' = 0$ and the (2,0) CN(A-X) band is ≈ 37 percent of the $v' = 2$ emission of CN(A) . A factor of two was applied to the intensity of the $\text{CN(A)}_{v'=2}$ emission to allow for quenching by C_2N_2 ($k = 7.3 \times 10^{-11} \text{ cm}^3 \text{ molecules}^{-1} \text{ s}^{-1}$, Ref. 50) and O_2 [k not known for $v' = 2$ but assumed to be $3 \times 10^{-11} \text{ cm}^3 \text{ molecules}^{-1} \text{ s}^{-1}$ as measured for $v' = 0$ and 1 in Ref. 52]. With 1-2 mJ of 158-nm radiation focused into the cell, the peak CN densities produced were estimated as $(5-10) \times 10^{14} \text{ molecules cm}^{-3}$, corresponding to considerable depletion of the initial C_2N_2 concentration, and γ -band quantum yields (i.e., γ -band photons per absorbed photon) as high as 5×10^{-3} were observed (with a factor of 3 estimated uncertainty). Figure 5 shows the calculated yields, with Reaction (15a) as the only $\text{N}_2(\text{A})$ source, for a $\text{C}_2\text{N}_2\text{-O}_2$ ($10^{15} \text{ molecules cm}^{-3}$) mixture. This graph shows a predicted γ -band yield of $\approx 5 \times 10^{-3}$ for $\text{CN} = 10^{15} \text{ molecules cm}^{-3}$. This yield would rise to $\approx 2.4 \times 10^{-2}$ if the C_2N_2 is completely bleached. The initial production of O by O_2 photodissociation at 158 nm reduces the γ -band yield in the bleached situation (from 2.4×10^{-2} to 1.9×10^{-2} for initial $[\text{O}] = 6 \times 10^{14} \text{ molecules cm}^{-3}$). Hence, Reaction (15a) producing $\text{N}_2(\text{A})$ with ≥ 25 percent yield can account for the yield observations (assuming that the rate coefficient is the $1 \times 10^{-10} \text{ cm}^3 \text{ molecules}^{-1} \text{ s}^{-1}$ used in the model). Calculations for $[\text{C}_2\text{N}_2] = [\text{O}_2]$ ($10^{15} \text{ molecules cm}^{-3}$) using Reaction (22) as the only $\text{N}_2(\text{A})$ source give a γ -band yield of 1.5×10^{-3} for $[\text{CN}] = 10^{15} \text{ molecules cm}^{-3}$. This value rises to 4.4×10^{-3} if the C_2N_2 is completely bleached. Hence, for Reaction (22) to be the $\text{N}_2(\text{A})$ source, not only would the C_2N_2 have to be completely bleached but the $\text{N}_2(\text{A})$ yield would have to be 100 percent. The situation is made even more difficult because the initial production of O by O_2 photodissociation reduces the γ -band yield in the bleached situation (from 4.4×10^{-3} to 3.3×10^{-3} for initial $[\text{O}] = 6 \times 10^{14} \text{ molecules cm}^{-3}$).

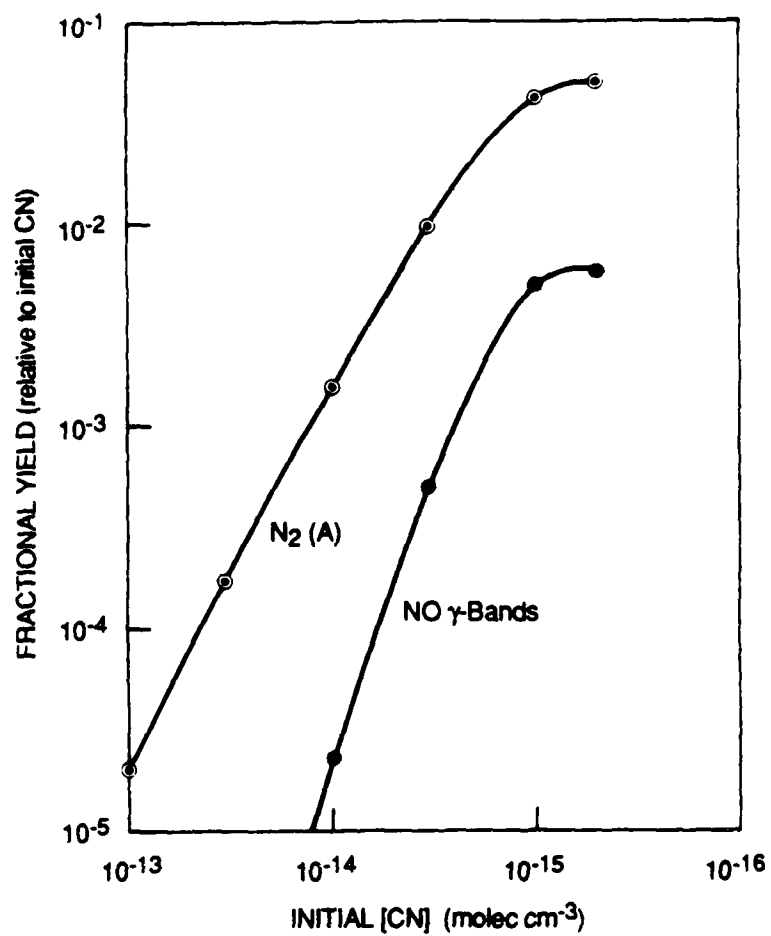


Figure 5. Model calculations of time-integrated yields of $N_2(A)$ and NO γ -bands as a function of initial CN concentration.
 $[C_2N_2] = 10^{15}$ molecules cm^{-3} , $[O_2] =$ molecules cm^{-3} .

Furthermore, the efficiency of Reaction (16) may not be the 100 percent assumed in this model. Also, if the energy pooling loss of $N_2(A)$ [Reaction (25) in Table 1] has a rate coefficient as high as $2 \times 10^{-9} \text{ cm}^3 \text{ molecules}^{-1} \text{ s}^{-1}$ (Ref. 53), this would reduce the γ -band yield in the bleached situation. Without bleaching, the effect is ≤ 10 percent on the γ -band yield because of the fast removal of $N_2(A)$ by C_2N_2 . Even with a higher rate coefficient for Reaction (22), it seems unlikely that Reaction (22) could account for all the γ -band yield, although such a contribution cannot be excluded.

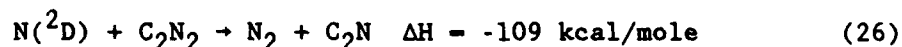
In fact, some yield might be anticipated from results (Ref. 54) on the isoelectronic reaction of $N(^4S) + N_3$ in which an ≈ 20 percent yield of $N_2(B^3\Pi_g)$ is formed. This emits first positive radiation to produce $N_2(A)$. In the present experiment, if the sole source of $N_2(A)$ was $N_2(B)$ and both Reactions (15a) and (22) are sufficiently exothermic to produce $N_2(B)$, 1+ emission would have been detected in the visible and IR regions despite the presence of the $CN(A \rightarrow X)$ emission in this region.

Additional evidence against an important contribution from Reaction (22) was found in the effect of NO on the γ -band yield. In Fig. 4, the experimental points were simply normalized to the computed curves so that the experimenters could look for differences in shapes. However, the relative yields of γ -bands are available from the experiments and show that small additions of NO enhance the γ -band emission, as expected from Reaction (16). The experiments also show that the enhancement (relative to no added NO) persists even at the highest NO addition ($1.76 \times 10^{15} \text{ molecules cm}^{-3}$). This is consistent with Reaction (15a) but not Reaction (22) as the $N_2(A)$ source because additional NO introduces a large additional loss of $N(^4S)$, whereas $N(^2D)$ is already being removed by C_2N_2 and therefore the effect of the additional removal by NO is mitigated.

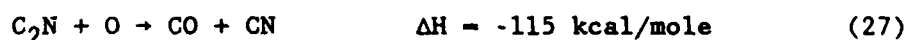
Thus, although none of the evidence is conclusive, it all points to Reaction (15a) as the important source of $N_2(A)$ and hence NO γ -band chemiluminescence in the photodissociated cyanogen-oxygen system.

It is interesting to note that the NO γ -bands are a very weak feature of the chemiluminescence produced in the photodissociated C_2N_2 - O_2 system. Clearly $CN(A$ and $B)$ and the triatomic emitters NCO , NCN , and CCN are more efficiently produced. In fact, from Fig. 1 and the relative monochromator-

photomultiplier sensitivity, it appears that the most intense chemiluminescent feature, CN(B) emission, has a quantum efficiency of ≥ 0.1 . It is interesting to speculate that, since a major loss of $N(^2D)$ is assumed to be reaction with C_2N_2 , if the reaction proceeds by



there is sufficient exothermicity to produce the observed $C_2N(A \rightarrow X)$ emission at 466 nm. Furthermore, C_2N will be very reactive and its reaction with the O atoms present



is sufficiently exothermic to produce the CN(A) and CN(B) that are observed. It is this same reaction that was invoked (Ref. 55) to explain the CN emissions observed when C_2N_2 is added to partially titrated active nitrogen (with NO giving oxygen atoms). Clearly, measurements of the type described here for the γ -bands and additional modeling studies would help to determine the chemiluminescent mechanisms for the other emissions.

Thus, the results of the experiments and computer modeling pointed to Reaction (15) as the main source of $N_2(A)$ and the resulting emission of NO γ -bands via Reaction (16). Furthermore, the efficiency for producing $N_2(A)$ must be high. If the rate coefficient is $1 \times 10^{-10} \text{ cm}^3 \text{ molecule}^{-1} \text{ s}^{-1}$, then the efficiency must be ≥ 25 percent (with an uncertainty of ~ 3). A lower rate coefficient would require a proportionately higher efficiency, and vice versa.

It was also concluded that efficient generation of $N_2(A)$ by the C_2N_2 -O₂ system would hinge on the production of high CN densities ($\geq 10^{15} \text{ molecules cm}^{-3}$). Such densities were achieved in the experimental work using a focused beam of 158-nm radiation. Clearly, chemical generation would be necessary in a practical laser system. Some simple systems that might fulfill this requirement are lean flames of cyanogen in oxygen or ozone.

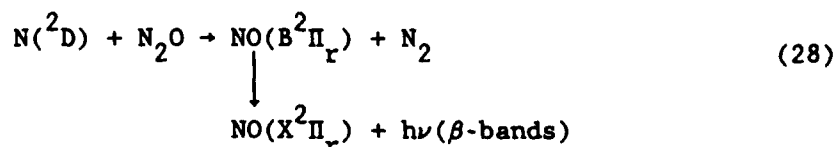
To further refine the findings of these pulsed photodissociation studies, some of the rate coefficients that had thus far only been estimated had to be measured. This need led to the search for a sensitive detector of $N(^2D)$,

which is of central importance in the $C_2N_2-O_2$ system and other systems being explored for their potential as chemical lasers. Such a detector was a necessary preliminary to kinetic studies of $N(^2D)$, and the resonance-enhanced multiphoton ionization (REMPI) technique proved a useful tool for this purpose.

4.0 REMPI DETECTION OF $N(^2D)$

4.1 INTRODUCTION

An important component of the earth's upper atmosphere, $N(^2D)$, is an intermediate in a number of visible chemical laser schemes presently under investigation. It is the first excited state of the nitrogen atom and lies 2.38 eV above the $N(^4S)$ ground state. Its radiative lifetime is 40 h. The $N(^2D_{5/2})$ and $N(^2D_{3/2})$ spin-orbit states are separated by 8 cm^{-1} . Laboratory studies of its quenching and reaction date back to 1969 (Ref. 56), when vacuum ultraviolet (vuv) photolysis of N_2O was used as its source and the NO β -bands produced by



were used to study the $N(^2D)$ kinetics. This work was followed by experiments using a microwave discharge of N_2 and rare-gas mixtures in a flow system (Ref. 57) as the source of $N(^2D)$ and line absorption at 149.3 nm to follow its kinetics. More recent work has added the techniques of resonance fluorescence (Refs. 9 and 58) and electron spin resonance (ESR) absorption (Ref. 59) to the detection repertoire.

Because working in this region is difficult in any case and becomes even harder in the presence of vuv absorbing gases like the C_2N_2 and O_2 of the present system, the REMPI technique was developed for studying $N(^2D)$. This technique was very useful in earlier studies of the metastable $S(^1D)$ species (Refs. 60-63). With it, it was possible to study the generation and removal of $S(^1D)$ in a variety of different systems. This study represents the first application of resonance-enhanced multiphoton ionization (REMPI) to the detection of $N(^2D)$. The technique has been applied to the detection of $N(^2D)$

in the products of a microwave discharge in N_2/Ar mixtures and in the products of two-photon absorption in N_2O at 269 nm.

The basis of the REMPI technique is shown in Fig. 6. Two-photon absorption by $N(^2D_J)$ at 269 nm produces the $3p\ ^2S^o$ state. A third photon can ionize this state or the state can decay radiatively by the emission of an infrared photon to produce the $3s\ ^2P$ state, the upper state in resonance absorption and fluorescence measurements of $N(^2D)$. The $3s\ ^2P$ state can then emit a vuv photon at either 149.3 or 174.2 nm: the former leaves the atom in the metastable $N(^2D)$ and the latter leaves it in the $N(^2P)$ state. This work has focused on the ionization channel because of the ultimate need to make measurements with gases that absorb strongly in the vuv region and because efficient photomultipliers are not available for the infrared emission.

4.2 EXPERIMENTAL METHOD

Most of the apparatus has been described in Ref. 64. The laser light source was a Quanta-Ray Nd:YAG dye laser that was operated with Exciton Coumarin 540A (pumped at 355 nm) to cover the 535-570-nm region. This beam was doubled (Inrad* Autotracker II) and then focused in the center of the cell with a 20-cm focal length lens (some measurements used a 35-cm focal length lens). The doubled light was ≈ 2 mJ. Stainless steel electrodes, ≈ 25 mm square, separated by 11 mm and biased with 90 V, were used to collect ions produced in the focal region. The collected ions passed to a charge-integrating preamplifier (Ortec** Model 113) and then to a boxcar averger and pen recorder recorder.

For the experiments with a microwave discharge, a 0.5-in. (1.27-cm) quartz tube passed from outside the cell and ended just above the laser focal region. To facilitate the transport of metastable species from the microwave discharge to the detection region, the small rotary pump normally used was replaced with a larger pump (Sargent-Welch*** DuoSeal Model 1402). With this pump, the transit time from the discharge to the detection region was ≈ 10 ms.

* Inrad, 181 Legrand Ave., Northvale, NJ 07647.

** Ortec, Inc., 100 Midland Rd., Oak Ridge, TN 37830.

*** Sargent-Welch, 7300 North Linder Ave., P.O. Box 183, Skokie, IL 60076.

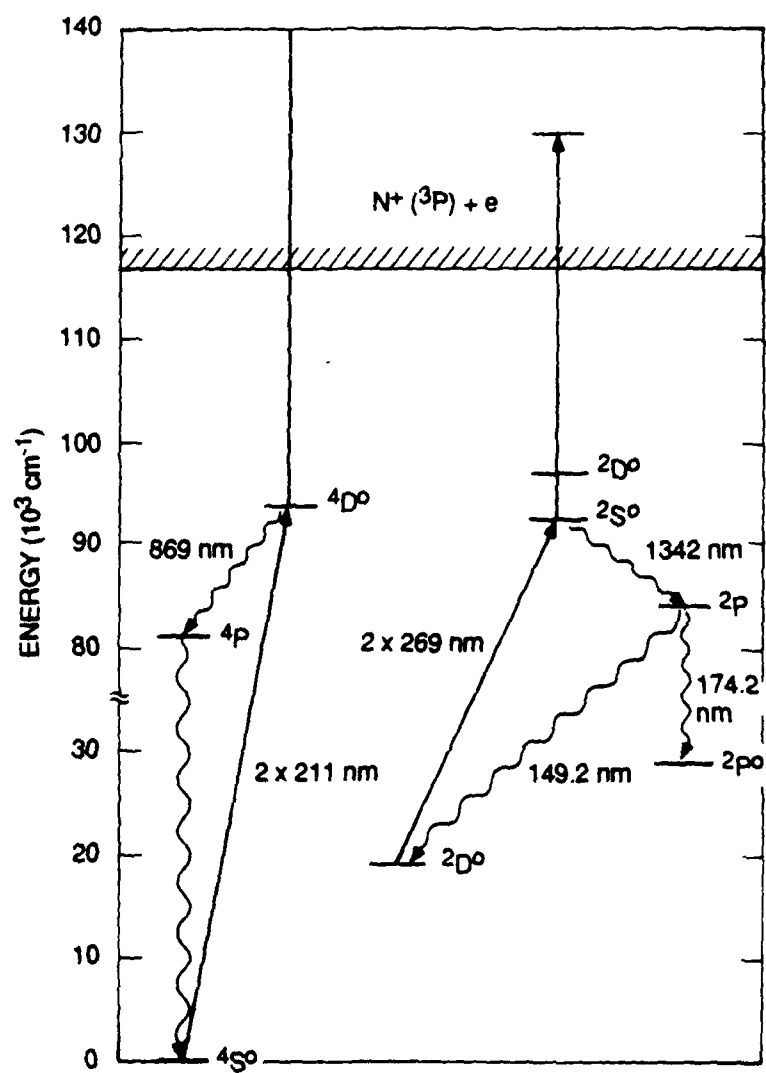


Figure 6. Two-photon absorption in $N(2D)$ and $N(4S)$ and subsequent ionization and emission processes.

The cell was equipped with MKS Baratron pressure gauges. The N_2O used was C.P. grade (99.0 percent minimum) and the Ar and N_2 were Prepurified grade (99.998 percent minimum).

4.3 RESULTS AND DISCUSSION

Figure 7 shows the $\text{N}(^2\text{D})$ signal detected ≈ 10 ms after a microwave discharge in 0.5 percent N_2 in argon at $\approx 3 \times 10^{17}$ molecules cm^{-3} . Similar signal levels were produced over a range of 0.2-2.0 percent N_2 in argon (at $\approx 3 \times 10^{17}$ molecules cm^{-3} total pressure). The signal was enhanced by increasing argon pressure. This enhancement strongly suggests that the dominant loss of $\text{N}(^2\text{D})$ is by wall deactivation over the ≈ 10 ms flow time between the discharge and the laser focal region. The signal occurs at the expected wavelength and exhibits the 8 cm^{-1} separation of the two spin-orbit states of $\text{N}(^2\text{D})$. A similar, although weaker, signal could be produced with no microwave discharge and only N_2O (at $\approx 3\text{-}6 \times 10^{16}$ molecules cm^{-3}) present. In this case, the $\text{N}(^2\text{D})$ must arise from two-photon absorption by the N_2O , and hence the photoionization signal is the result of the absorption of five photons. This process is very similar to the production of $\text{S}(^1\text{D})$ from CS_2 and its photoionization using 288 nm photons reported earlier (Ref. 65). Two photons at 269 nm access the same energy region in N_2O , where single-photon absorption produces a very low yield (Ref. 66) (≤ 1 percent) of $\text{N}(^2\text{D})$ from N_2O . Because the two-photon absorption may access a different initial state, the yield may be different even for the same energy input by the photon (or photons).

With the microwave discharge source, increasing the N_2 above ≈ 2 percent resulted in a decreasing $\text{N}(^2\text{D})$ signal. This was expected because of the quenching (Ref. 67) of $\text{N}(^2\text{D})$ by N_2 . With only N_2 through the microwave discharge, no $\text{N}(^2\text{D})$ lines could be seen but a molecular ionization spectrum was obtained. A portion of this spectrum between 533 and 542 nm is shown in Fig. 8. The feature marked (3,0), a Lyman-Birge-Hopfield (LBH) band, is producing an ionization signal via two-photon absorption at 270 nm from the ground state to the $a^1\Pi_g$ state of N_2 (the upper state of the LBH system) followed by two-photon ionization. Fluorescence and two-photon ionization from the $a^1\Pi_g$ state, also produced by two-photon absorption, have been

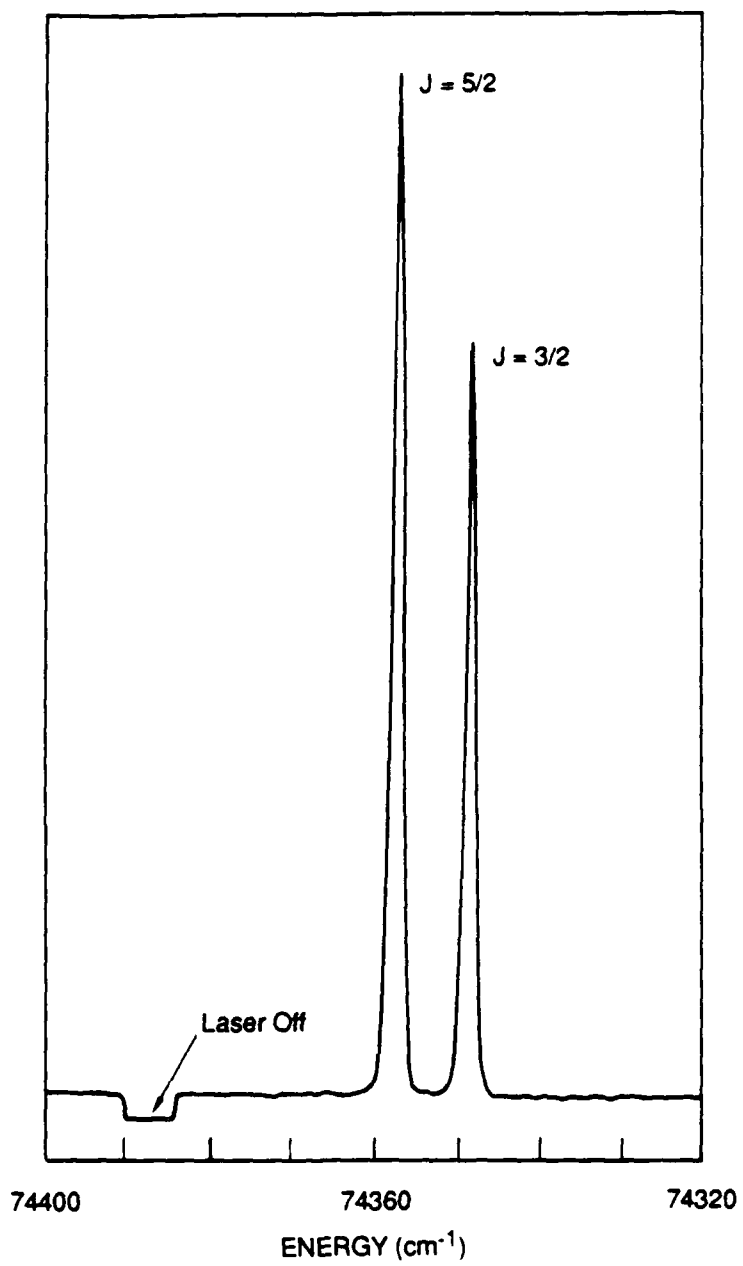


Figure 7. Three-photon (two to resonance) ionization spectrum from N(²D).

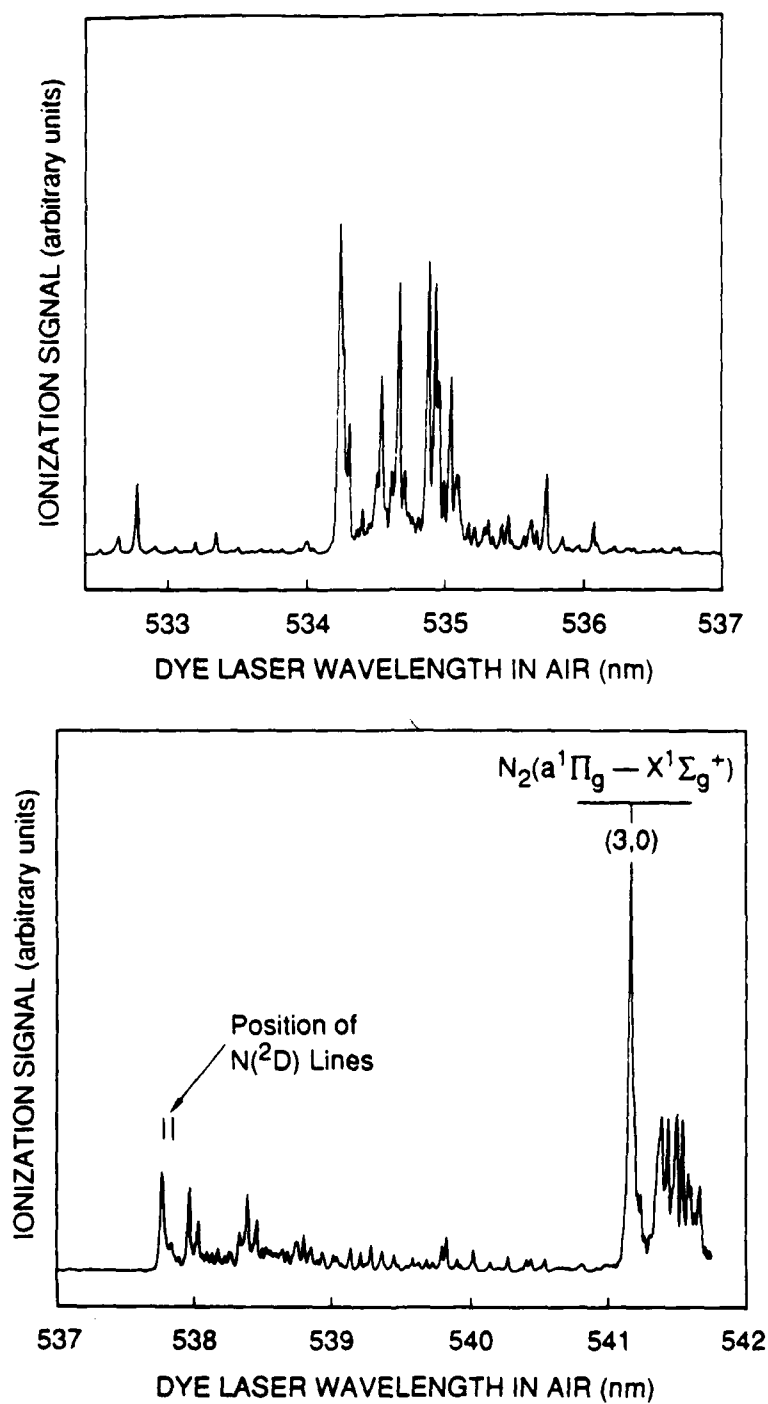


Figure 8. Resonance ionization spectrum of N₂ subjected to a microwave discharge versus dye laser wavelength in air (533 to 542 nm).
 [N₂] = 10¹⁷ molecules cm⁻³, flow time = 10 ms.

reported previously (Refs. 68 and 69). The assignment of the other two molecular features is not known, but they are only present when the discharge is on. The rotational structure clearly shows the presence of an intermediate resonance, and the strength of the signals (the dye laser power was ≈ 1.5 mJ/pulse and did not change significantly over the wavelength range of Fig. 8) suggests that the excitation and ionization involves fewer photons than the 2+2 involved in ionization of the ground state via the $a^1\Pi_g$ state. Because the structure of the two unknown bands is different from that of the LBH band, excitation and ionization of vibrationally excited N_2 via the $a^1\Pi_g$ state is probably not their source. A more likely source is an electronically excited metastable state or states of N_2 . The lowest three are the $A^3\Sigma_u^+$, $W^3\Delta_u$, and $a'^1\Sigma_u^-$ states (Ref. 70). Whereas the vibrational ground state of the $A^3\Sigma_u^+$ would require a total of three UV photons for ionization, the $W^3\Delta_u$ and $a'^1\Sigma_u^-$ states could undergo 1+1 photoionization. However, absorptions from the $W^3\Delta_u$ state are not known, and known transitions from the $a'^1\Sigma_u^-$ state cannot account for the features in Fig. 8. Table 2 gives the dye laser wavelengths at the band heads shown in Fig. 8 and those appearing in a scan covering longer wavelengths (to 570 nm). The identification of these bands is discussed in Section 6.

TABLE 2. Dye laser wavelengths in air (nm) of bandheads (± 0.1 nm) observed in REMPI of N_2 passed through a microwave discharge (in the region 534-570 nm).

534.2		555.3	
537.8		558.3	
541.2	[LBH (3,0)]	561.1	
544.4		564.8	
548.9		566.2	[LBH (1,0)]
552.1		568.0	
553.4	[LBH (2,0)]		

5.0 KINETICS STUDIES OF $N(^2D)$

5.1 INTRODUCTION

Studies of the reactivity of $N(^2D)$ are complicated by the fact that it is a difficult species to produce, transport, and monitor. It has been generated in N_2 discharges (Refs. 39, 57, 58) by vuv photolysis of N_2O , (Refs. 66, 71, and 72) and by photodissociation of $ClNCO$ (Ref. 73). Although it is an electronically excited state, its radiative lifetime of 10^5 s is the longest of any species known and obviously precludes its laboratory detection by photolytic methods; its radiation is only observed in the upper atmosphere. It has been detected by resonance absorption/fluorescence at 149.2 nm (Refs. 39, 57, 58, and 72), by ESR absorption (Ref. 59), and by the reaction with N_2O , which generates the $NO(B^2\Pi)$ state and thereby gives rise to NO β -band emission (Refs. 66, 71, and 73).

As was described in Section 4 above and Ref. 74 $N(^2D)$ can be detected by REMPI. The first allowed two-photon transition available to an $N(^2D)$ atom (Ref. 75) is to the $3p^2S^0_{1/2}$ state, at 93582.3 cm^{-1} . The two $N(^2D)$ levels, separated by 8.7 cm^{-1} , result in two transitions, at 74357.06 and 74348.34 cm^{-1} . For a two-photon process, radiation at 269 nm is therefore required. In principle, one can then detect $^2S\text{-}^2P$ emission at $1.3\text{ }\mu\text{m}$, but for this experiment the N^+ ion resulting from absorption of a third photon was monitored. In this study, $N(^2D)$ was generated in a N_2/Ar microwave discharge and monitored a few milliseconds downstream in an ionization chamber. The details of this process are described in Section 4.

The authors have recently reported (Ref. 76) on a system in which C_2N_2 and O_2 were simultaneously photodissociated, resulting in production of a number of radicals and excited states. The $NO(A^2\Sigma^+)$ state is one of the products, and its temporal behavior following the laser dissociation pulse was modeled. Another product, $N(^2D)$, arises from the interaction between CN and $O(^3P)$ and one of the important reactions whose rate coefficient required estimation was the quenching of $N(^2D)$ by C_2N_2 . A value of $7 \times 10^{-11}\text{ cm}^3\text{ molecule}^{-1}\text{ s}^{-1}$ was chosen. When this new way to study $N(^2D)$ was developed,

it was decided to test it on this reaction and at the same time make comparisons with known reactions.

5.2 EXPERIMENTAL METHOD

The technique involves generation of $N(^2D)$ in a 10-mm-I.D. quartz tube in which the flow velocity is 2 cm/ms. The quenching gas is introduced into the yellow afterglow, where the residence time is 6.7 ms. The quartz tube exits into the ionization cell, at which point two plates, both biased positive with respect to the cell walls, and with 90 V across them, collect ions. The region is irradiated by a focused Nd:YAG-pumped dye laser operating at 10 Hz, at close to 269 nm, and the ion current is collected and processed, as described in Section 4.

It was found necessary to cool the quartz tube between the quencher addition point and the entrance to the cell. This was done with water circulating through a Tygon coil. Thermocouples on the tube both inside and outside the ionization cell were thus maintained at 300 K.

5.3 RESULTS AND DISCUSSION

The inset in Fig. 9 shows the signal resulting from the three-photon process. The optimum pressure was found to be 1 percent N_2 in Ar at 10 torr. At higher N_2 , other features develop in the ion signal. Two-photon-excited N_2 LBH bands from $N_2(X) v = 0$ have been observed as well as other bands which appear to require excited N_2 , but those have not yet been identified. At higher pressures of Ar, the $N(^2D)$ signals get very large, but there is evidence that a second source is thereby created and $N(^2D)$ is formed throughout the flow tube.

The quenching data consist of measuring the $N(^2D)$ signal, I , as a function of added reactant, Q , where the contact time, τ_f , and concentrations are related by

$$\ln(I/I_0) = -\tau_f k_Q [Q] \quad (29)$$

where I_0 is the signal in the absence of added reactant and k_Q the quenching rate coefficient. The contact time can require a correction for parabolic

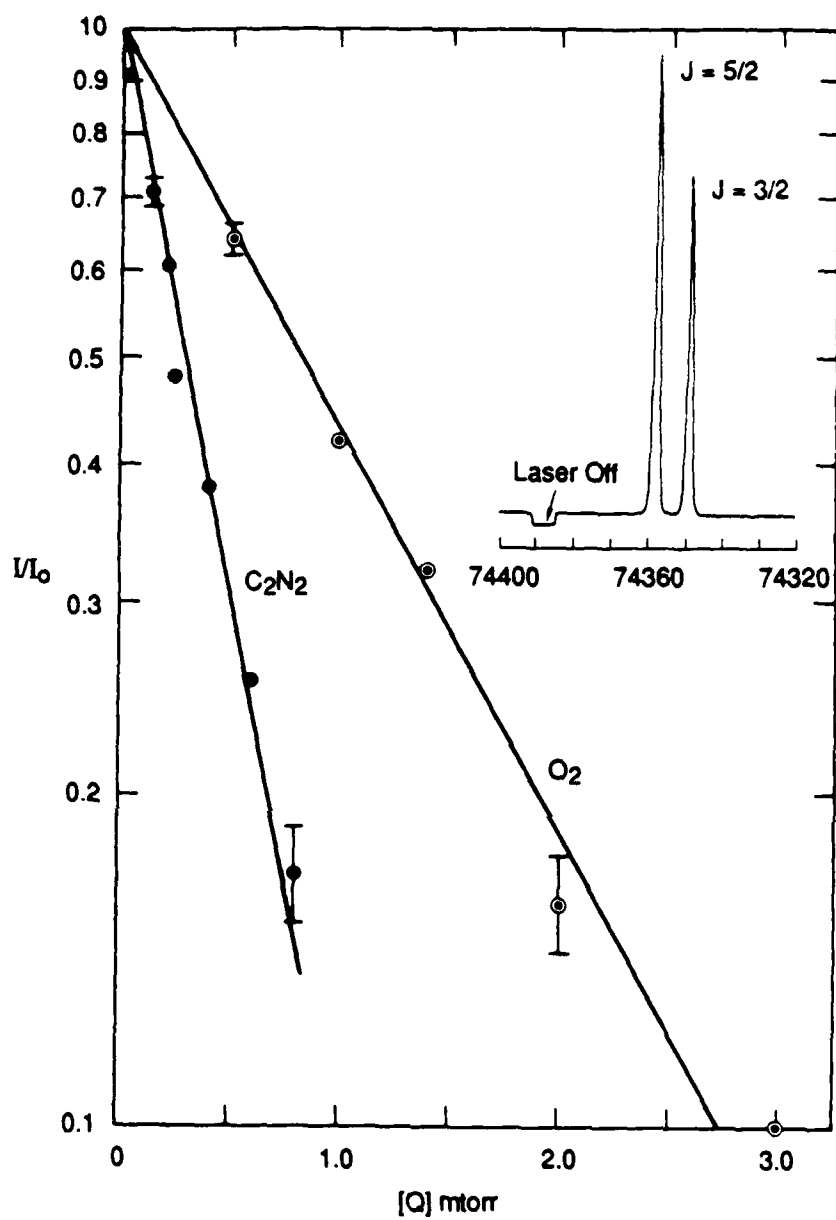


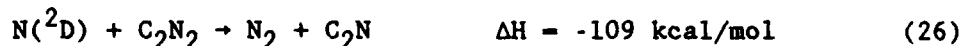
Figure 9. I/I_0 versus $[Q]$ for $Q = O_2, C_2N_2$.
 $T = 300$ K, contact time = 6.7 ms.

flow. From measurements on a calibrated volume and the tube length, its average value was determined to be 6.7 ms.

Values for I and I_0 were obtained by establishing a signal level (I_1), adding the quencher to obtain I_2 , shifting the laser wavelength to a fixed off-resonance position (I_3), then turning off the quenching gas (I_4). I_0 is then $I_1 - I_4$, and I is $I_2 - I_3$. This procedure was required because of the possibility of the quenchers giving a background ion signal.

The data for C_2N_2 and the standard quencher, O_2 , are presented in Fig. 9. Both C_2N_2 and O_2 were both added as analyzed 1 percent mixtures in Ar. The $1/e$ quenching pressure for C_2N_2 is 0.42 mtorr, that for O_2 is 1.18 mtorr, and from Equation (29) the values of k_Q for C_2N_2 of $1.12 \times 10^{-11} \text{ cm}^3 \text{ molecule}^{-1} \text{ s}^{-1}$ and for O_2 of $3.97 \times 10^{-12} \text{ cm}^3 \text{ molecule}^{-1} \text{ s}^{-1}$ are found. The ratio is 2.81. The results obtained by M. P. Iannuzzi and F. Kaufman in a similar study of the $N(^2D) + O_2$ reaction (Ref. 58) agreed with the experimenter's value. Using argon as the carrier and 149.2-nm absorption for $N(^2D)$ detection, an uncorrected value of $(4.01 \pm 0.23) \times 10^{12} \text{ cm}^3 \text{ molecule}^{-1} \text{ s}^{-1}$ for the rate coefficient was obtained. After a parabolic flow correction for argon, the absolute value for k_{O_2} was $(5.49 \pm 0.32) \times 10^{-12} \text{ cm}^3 \text{ molecule}^{-1} \text{ s}^{-1}$, which agreed with other determinations (Refs. 39, 57, 59, 71, and 72). When the same correction is applied to this study's data, the value for the C_2N_2 rate coefficient at 300 K becomes $(1.5 \pm 0.2) \times 10^{-11} \text{ cm}^3 \text{ molecule}^{-1} \text{ s}^{-1}$, a factor of 4.5 smaller than previously estimated (Ref. 76). The error limits arise from the precision of the data in Fig. 9.

In the earlier work on C_2N_2/O_2 (see Section 3), the $N(^2D)/C_2N_2$ interaction was assumed to be reactive:



This reaction is sufficiently exothermic to produce C_2N in its A state. In fact, both ground and A state C_2N have been detected in photolyzed C_2N_2/O_2 and their temporal profiles have been measured (the A-X emission is at 466 nm). Unfortunately, the temporal profile of $N(^2D)$ has not yet been determined, so the role of Reaction (26) in producing the observed C_2N is still uncertain. There is hope that the REMPI technique will lead to clarification of the role of $N(^2D)$ in C_2N production.

6.0 REMPI STUDIES IN THE LEWIS-RAYLEIGH AFTERGLOW OF NITROGEN

6.1 INTRODUCTION

In the spring of 1987, Dr. Black was invited to be a visiting professor at the Institute for Molecular Science in Okazaki, Japan. This visit provided an opportunity to explore the origin of the series of molecular bands observed in the REMPI studies of microwave-discharged nitrogen reported in Section 4. At that time, the signals were thought to originate from electronically excited metastable states of N_2 . The studies performed in Japan indicate that the molecular features observed in the earlier work more probably arise from highly vibrationally excited nitrogen species possessing over $50,000\text{ cm}^{-1}$ of vibrational energy. Such species are roughly isoenergetic with $N_2(A^3\Sigma_u^+)$ and may be coupled to this state through nitrogen atom exchange. Studies of the energy flow in this system and the role played by $N_2(A^3\Sigma_u^+)$ must take the presence of these species into account. The work both at SRI and in Japan shows that the REMPI technique is sensitive enough to apply to the study of these species and much more convenient than the alternative, vuv absorption.

The presence of vibrationally excited molecules (up to $v'' = 29$) in the pink and Lewis-Rayleigh afterglow of nitrogen has been known for a long time (Refs. 77 and 78). These were detected by vuv absorption methods that also detected (Ref. 79) the metastable $^2D^o$ and $^2P^o$ states of the nitrogen atom. In the work discussed in Section 4, $N(^2D^o)$ was detected using the REMPI technique at 269 nm (using a 2+1 process) in dilute (0.2-2 percent) nitrogen in argon mixtures. When the argon was replaced by nitrogen, the metastable $N(^2D^o)$ atom signal disappeared and a number of molecular features were observed, the most obvious of which were REMPI signals produced from $N_2(v'' = 0)$ by 2+2 photoionization via the $a^1\Pi_g$ state (a two-photon allowed transition from the ground state). Such transitions have been detected previously both by observing fluorescence (Ref. 68) from the intermediate $a^1\Pi_g$ state and by observing the photoelectrons produced (Ref. 69).

A number of other unassigned REMPI transitions were observed only when the microwave discharge was operating. The most likely source of these additional features is now thought to be the highly vibrationally excited

nitrogen observed in the earlier work (Refs. 77 and 78), because in this work, at slightly shorter wavelengths, the presence of highly vibrationally excited N_2 with over $50,000\text{ cm}^{-1}$ of vibrational energy ($v'' = 26$) is demonstrated using the REMPI technique.

6.2 EXPERIMENTAL METHOD

The laser light for these experiments was obtained from an excimer pumped dye laser (Lumonics,* HyperEX-400 and HyperDYE-300) that was doubled (HyperTRAK-1000). Using Coumarin 500 allowed generation of wavelengths in the range of 244 to 263 nm with pulse energies of ~ 0.1 to ~ 1.5 mJ. Some preliminary experiments used Coumarin 540 to cover 267 to 285 nm. This light passed through a focusing lens ($f = 15$ cm) and into a square metal cell (a volume of 1 L) through a plane quartz window. The laser focus was between two metal plates separated by 10 mm and biased at +90 V and +180 V. (Keeping both plates positive greatly reduced interference from ions in the afterglow.) The collected ions passed through a 1-kHz filter (to further reduce interference by the microwave-generated ions) to a charge-integrating preamplifier (Ortec Model 113) and then to a boxcar averager and pen recorder.

The metal cell was part of a fast flow gas system using 12-mm-I.D. Pyrex tubing in which the linear velocity was ~ 60 m/s. The tubing passed into the cell, and the gas flow exited the Pyrex tubing just before the laser interaction region. A microwave discharge (EWIG, MR-301) was operated at varying distances from the cell (corresponding to flow times of 2-6 ms). Gases could be added at several addition points between the discharge and the metal cell. The cell was equipped with a MKS pressure gauge. The N_2 and Ar used were of 99.999 percent purity, and the CO_2 used to quench the vibrationally excited nitrogen was of 99.9 percent purity.

* Lumonics Inc., 105 Schneider Rd., Kanata (Ottawa), Ontario, Canada K2K 1V3

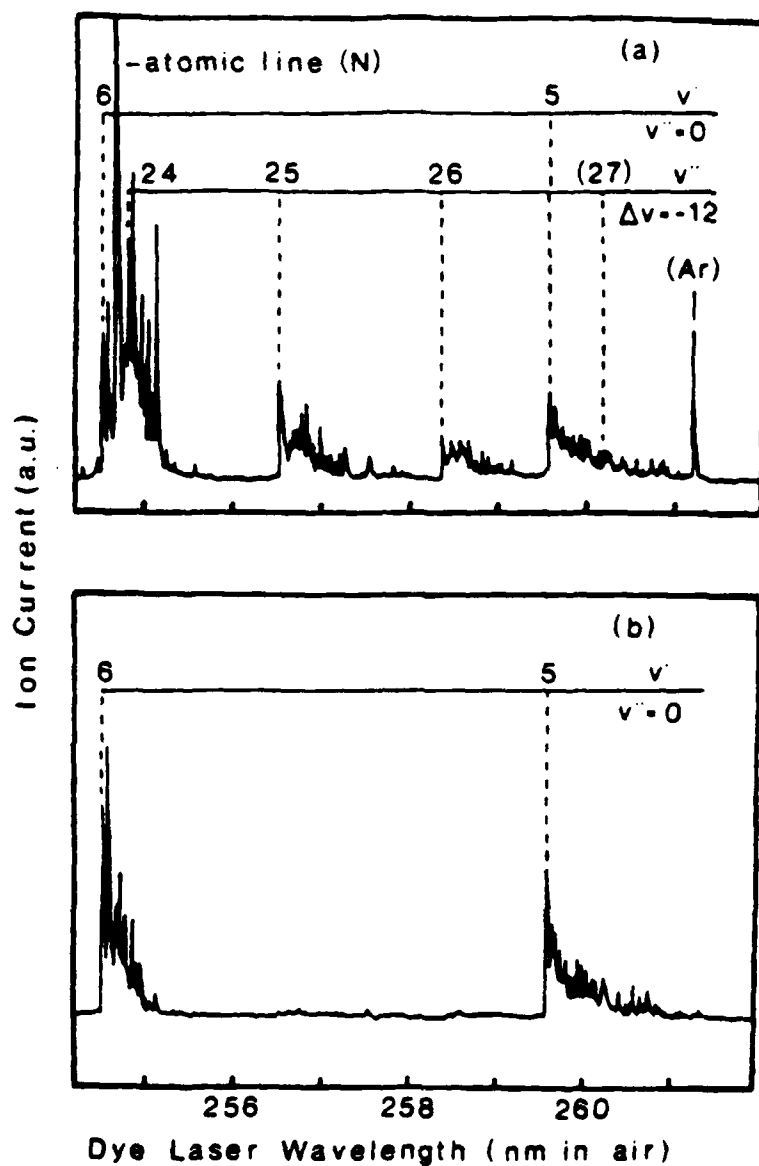
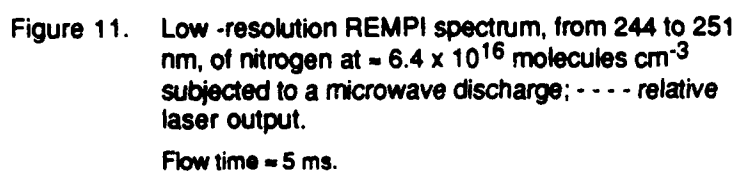


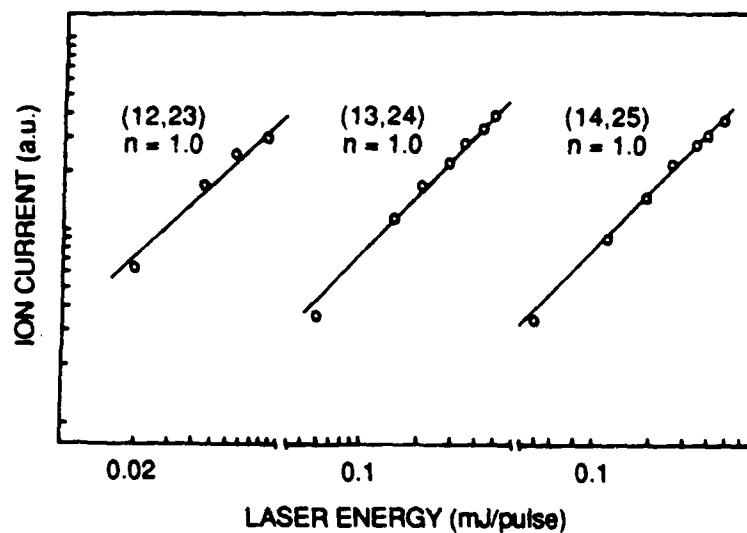
Figure 10. (a) Low-resolution REMPI spectrum, from 254.2 to 262 nm, of a 4:1 N₂:Ar mixture at a total pressure of $\approx 7.7 \times 10^{16}$ molecules cm⁻³ when subjected to a microwave discharge. Flow time = 5 ms. (b) Effect of replacing Ar by CO₂ (added after the discharge) in the above experiment.

6.3 RESULTS AND DISCUSSION

In the absence of the discharge, the (2+2) REMPI spectrum of N_2 ($v'' = 0$) reported in Refs. 68 and 69 was obtained. Ionization via the $a^1\Pi_g$, $v'' = 2, 3, 5, 6$, and 7 was observed. When the discharge was on, the well-known Lewis-Rayleigh afterglow and a number of additional features appeared. Figure 10(a), obtained with a 4:1 N_2 /Ar mixture at a total pressure of 7.7×10^{16} molecules cm^{-3} , shows the region from 254.2 to 262 nm, in which the additional features are assigned as ionization via the (12,24), (13,25), (14,26), and possibly the (15,27) LBH transitions of $N_2(a^1\Pi_g \leftarrow X^1\Sigma_g^+)$. These wavelength assignments were made on the basis of the review of A. Lofthus and P. H. Krupenie (Ref. 70). Over this region the laser pulse energy was approximately constant. Two atomic lines are seen in this region. The longer wavelength one is only produced when the argon is present and therefore arises from this atom. The shorter wavelength line is present even with no argon addition and therefore presumably arises from atomic nitrogen (although neither feature could be assigned). A number of additional experiments were performed to confirm the assignments of the molecular features. The replacement of argon by CO_2 (adding the CO_2 after the discharge) resulted in the spectrum shown in Fig. 10(b). This spectrum is the same as that obtained in the absence of the discharge and shows only the (6,0) and (5,0) LBH transitions. The atomic line contamination of the (6,0) band was also removed by the CO_2 addition. Efficient removal of nitrogen vibrational energy by CO_2 is well known (it is the basis of the CO_2 10- μm laser), so this observation is consistent with the assignments shown.

Figure 11 shows the region from 244 to 251 nm. In this region, the bands assigned to the $\Delta v = -11$ sequence ($v'' = 23, 24$, and 25) become much stronger than the transitions associated with $N_2(v'' = 0)$. In fact, only the (7,0) transition is clearly seen, whereas at the position of the (8,0) band, any signal is close to the noise level of the experiment. In this region the laser output varies with wavelength, as shown in Fig. 11. The intensities observed here can be explained by the power dependences of the signals, which are shown in Figs. 12 and 13. Whereas the bands of the $\Delta v = -11$ sequence show a linear dependence on laser pulse energy (Fig. 12), the bands originating on $N_2(v'' = 0)$ show a much higher dependence on laser pulse energy (where n is the exponent of that dependence). Hence, where the laser pulse energy is lowest,





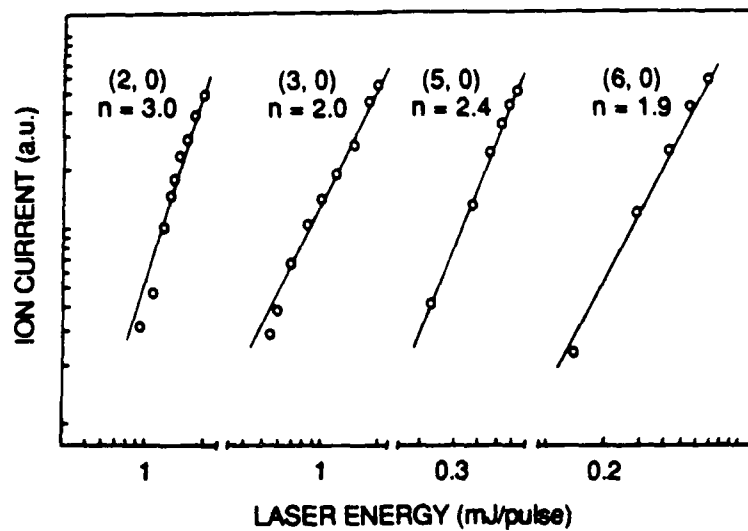


Figure 13. Power dependencies of the ionization signals arising through the excitation of the (6, 0), (5, 0) and (3, 0) and 2, 0) LBH transitions in nitrogen at $\sim 6.4 \times 10^{16}$ molecules cm^{-3} .

only transitions involving the highly vibrationally excited nitrogen are seen. This is the situation at the shortest wavelengths in Fig. 11.

For the $\Delta v = -11$ sequence of transition from $v'' = 23, 24$, and 25 levels, the photoionization will involve a $1+1$ REMPI process, so the linear dependence on laser power implies that either the excitation of the $a^1\Pi_g$ state or its subsequent ionization is saturated under these conditions. The former seems most likely. The weak transitions shown in the $\Delta v = -12$ sequence for $v'' = 19, 20$, and 21 can only arise by a $1+2$ REMPI process, and hence the weak signals will reflect the much smaller cross section for a three-photon process (in comparison to that for a two-photon process) and does not imply that the $v'' = 19, 20$, and 21 levels have much smaller populations than the $v'' = 23, 24$, and 25 levels. The LBH transitions from $N_2(v'' = 0)$ to $v' = 2-7$ must all involve a $2+2$ REMPI process, yet the results in Fig. 13 show that the power dependences are quite variable and must reflect the effects of saturation at some of the excitation or ionization steps. When $n = -2$, it seems likely that the two-photon absorption step is being saturated (since it is a fully allowed two-photon transition) and the residual power dependence is that of the ionization process. The effects of saturation on a $2+2$ ionization process, at the moderate fluences of these experiments (10^{27} - 10^{29} photons $\text{cm}^{-2} \text{s}^{-1}$), have been discussed previously (Ref. 80).

In light of these results, it seems likely that the molecular features observed in the earlier work (see Section 4) between 265 and 285 nm arise from the same source, that is, highly vibrationally excited nitrogen. Unfortunately, tabulations (Ref. 70) of transitions for vibrationally excited nitrogen do not extend beyond 260.2 nm [the $(15,27)$ LBH band]. Knowledge of the energy levels of very highly vibrationally excited nitrogen should increase with additional careful analysis of the long wavelength bands, combined with spectral simulation.

7.0 PHOTOLYTIC SOURCES OF $N(^2D)$

7.1 INTRODUCTION

The radiative lifetime of $N(^2D)$ has been calculated as 10^5 s (Ref. 81). Except at high thermospheric altitudes, radiation from $N(^2D)$ is never detected, because quenching is invariably many orders of magnitude faster than the radiative rate. There are a variety of ways to produce $N(^2D)$ in gas discharges and in atmospheric processes. Reaction with O_2 produces vibrationally excited NO (Ref. 82), and current atmospheric models include this reaction as the principal source of thermospheric NO (Ref. 83).

In the studies described in Sections 4 and 5, REMPI proved to be a technique with very good sensitivity for $N(^2D)$. For this metastable atom, a 2+1 process, involving two photons at 269 nm that are absorbed by the $N(^2D^0)$ doublet to reach the $^2S^0$ level (Ref. 75) at 93581.52 cm^{-1} , leads to ionization. The method was subsequently applied to determining rate coefficients for reaction of $N(^2D)$ with C_2N_2 (Ref. 84) and with $O(^3P)$ (Ref. 85). The rate coefficient with $O(^3P)$ has been a source of considerable controversy in thermospheric chemistry (Refs. 39 and 83).

During the kinetic studies of $N(^2D)$ described in Section 5, it became apparent that the probing radiation at 269 nm gave the characteristic $N(^2D)$ doublet ion signal not only from the $N(^2D)$ atoms in the afterglow (i.e., in the presence of an N-atom stream) but also from photodissociation of NO and N_2O . The two-photon wavelength limit for producing $N(^2D)$ from NO is 279 nm, so the process probably involves two-photon absorption by NO, followed by direct dissociation or predissociation. Detection then requires three photons, so five photons in all are used. The process is shown schematically in Fig. 14. Because there is no reason to believe that this mechanism, whatever its detailed nature, is most effective at precisely the wavelength of the resonant transition in $N(^2D)$, an experiment was set up incorporating two dye lasers to decouple production from detection and to investigate the wavelength dependence of $N(^2D)$ production from NO. The plan was to

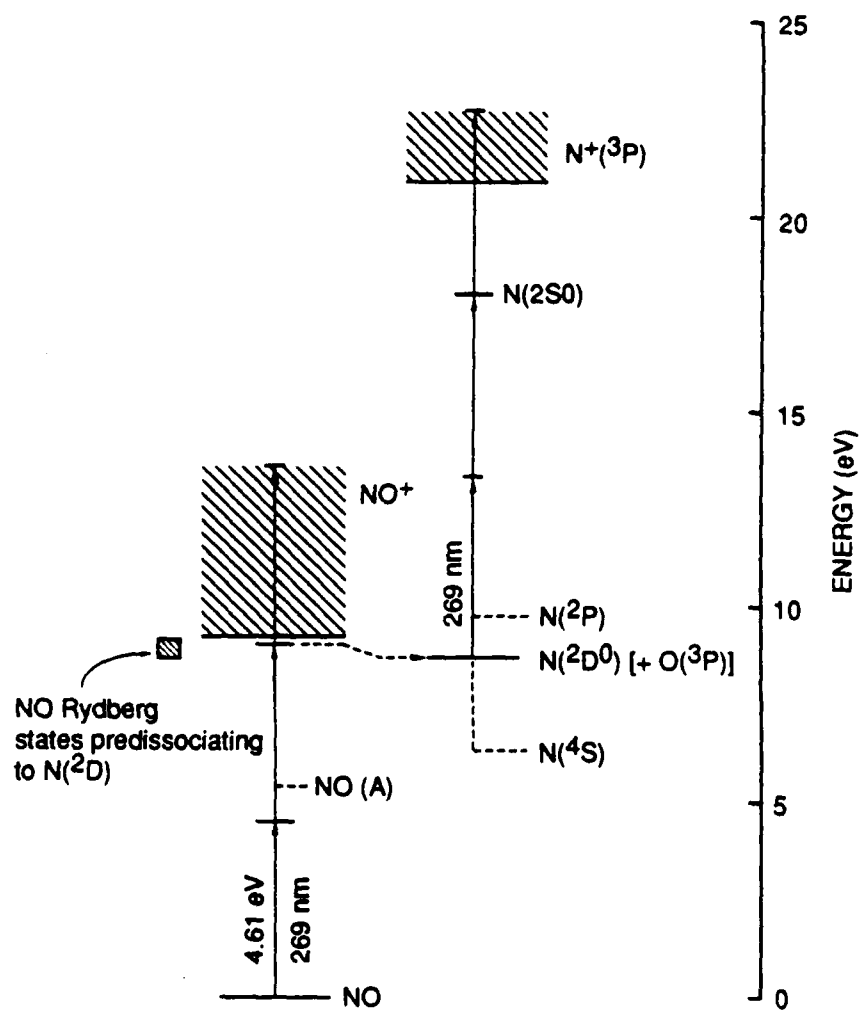


Figure 14. Schematic representation of multiphoton processes.

investigate photodissociation of NO in the energy region between 8.89 eV [the energy required to produce $N(^2D) + O(^3P)$] and 9.26 eV (the ionization limit).

7.2 EXPERIMENTAL METHOD

Two separate Nd:YAG-pumped dye lasers were used for the experiments, a Quanta-Ray DCR/PDL and a Quantel YG580/TDL 50. The 269-nm radiation needed to detect $N(^2D)$ was generated by doubling 538-nm radiation produced by 355-nm pumping of Coumarin 540A. The same system was used in the second laser for NO dissociation below 272 nm. At longer wavelengths, 532-nm pumping of Fluorescein 548 was much more efficient. Typical laser intensities were 2-5 mJ for Coumarin 540A and 10-15 mJ for Fluorescein 548. Both beams were focused into the cell with 50-cm lenses. The lasers were externally triggered by an SRS 535A delay generator, and ions were collected with an EG&G Ortec Model 113 charge integrating amplifier, processed through an SRS 250 boxcar averager, and displayed on a chart recorder. The electrodes were separated by 1 cm and biased at +180 V.

The two-laser production and detection of $N(^2D)$ from NO requires two focused laser beams, and thus the overlap of the counterpropagating beams is a critical issue. Each beam had a diameter of $\sim 150 \mu\text{m}$ at its focus, and the easiest way to align the beams was to burn a hole in a piece of metal foil with one laser, at the focal point, and then adjust the second laser to pass through the hole. This was adequate for the initial alignment; then in the evacuated cell, the arrangement was optimized by two-color excitation of discharge-produced $N(^2D)$. In this case, one laser was set at the two-photon transition frequency minus $\Delta\nu$ and the second laser at the transition frequency plus $\Delta\nu$. A signal could only be detected when the beams interacted, and the correct geometry was assured. Subsequently, when the wavelengths for producing high $N(^2D)$ yields were learned, this information could also be used in aligning the beams. Wavelength calibration of the system was simplified with accurate knowledge of the $N(^2D)$ detection wavelength and also with the aid of the REMPI signals generated from photodissociation of NO_2 , which produces vibrationally excited NO and thus leads to ion signals at $\text{NO}(A-X)$ band transition frequencies (Ref. 86).

The NO employed was a 10 percent mixture in He, used without further purification. The most likely impurity is NO₂, the presence of which is very noticeable if there is any air leak into the system, because of the resulting strong ion signals. After the regions of enhanced N(²D) production were found, contaminant signals originating from NO₂ were negligible.

The experiment was conducted by setting the narrow-line Quantel (Q) laser at the 2-hν transition wavelength of 269 nm and scanning the Quanta Ray (QR) laser. At times, QR was set at 269 nm or 270 nm and Q was scanned.

7.3 RESULTS AND DISCUSSION

The 2-hν threshold-to-ionization range is 279-267 nm, and within this region the enhancement of the N(²D) ion signal over that obtained with a one-laser scan at 269 nm was particularly large around 270 nm. Figure 15 shows two spectra: in the lower one, a REMPI scan with QR, the detected ion signal is from NO⁺ everywhere except at 269 nm, the N(²D) transition frequency; in the upper spectrum Q is set at 269 nm and QR is again scanned. The spectral features are approximately the same in the two spectra, but the much greater amplitude of the upper spectrum represents the N(²D) yield throughout this spectral region, which in the absence of the second laser does not produce an ion signal. If the ions were analyzed with a mass spectrometer, it would be evident that the enhanced spectrum is composed of the NO⁺ signal from the lower spectrum plus the N⁺ signal from the 2+1 ionization of N(²D).

The small signal at 269 nm demonstrates that N(²D) production at that wavelength is relatively small. The experimenters were quite fortunate to detect it in a one-laser experiment, because that wavelength is barely in the tail of the band. To compare the N(²D) yield at the detection frequency (269 nm) with the yield at the peak of the band (270 nm), QR was set at each of the two frequencies and Q was scanned. After subtraction of the Q contribution, the N(²D) doublet signal at 270 nm was found to be a factor of 50 larger than that at the N(²D) resonant frequency, so there is clearly a large range of yields over a limited spectral region.

The two spectra in Fig. 15 are basically identical, and the similarities provide information about the nature of the NO^{*} state. It is evidently not a

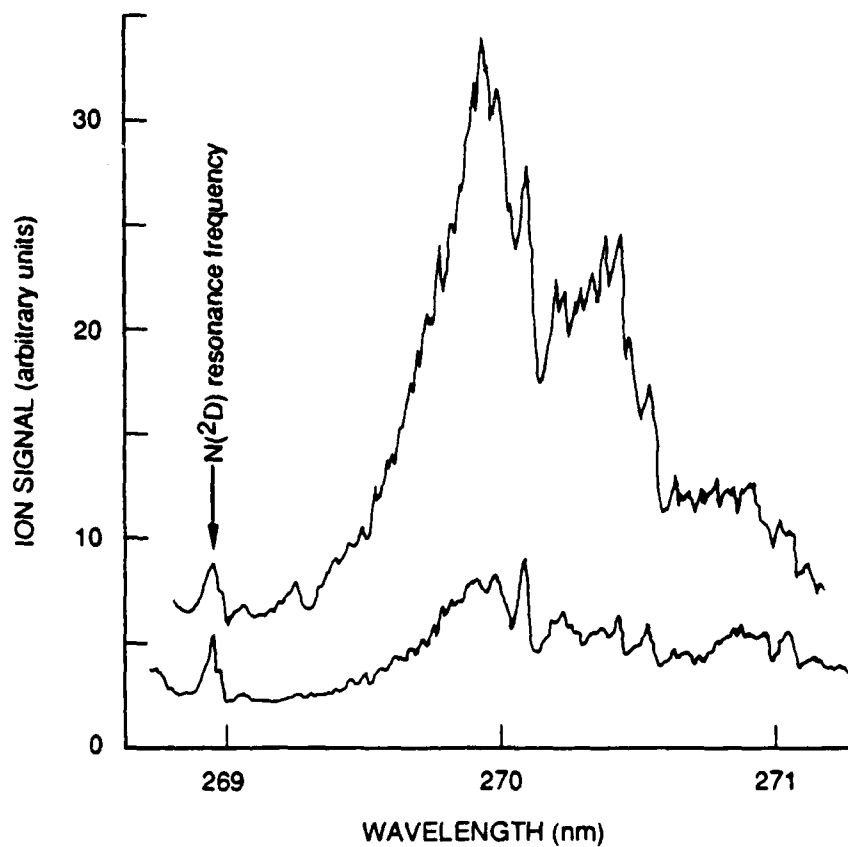


Figure 15. QR scan with Q (upper plot) and without Q (lower plot) [NO] = 25 torr, [He] = 5 torr, Q laser set at $N(^2D^{\circ})_{5/2} \rightarrow N(^2S^{\circ})$ resonance frequency, 10 ns delay between lasers, $I_{QR} = 3$ mJ, $I_Q = 3$ mJ.

purely dissociative state, because in that case its lifetime would not be long enough for absorption of a third photon and detection of ionization. Neither is it a state that only decays by radiation, because then $N(^2D)$ would not be produced. NO^* must be a predissociating state, with a lifetime long enough for absorption of an ionizing photon. Furthermore, the almost perfect correlation between the two spectra suggests that a single NO^* state is involved, because for a given laser power, the production ratio of NO^+ to $N(^2D)$ is invariant.

Figure 15 shows that the ion signal in the presence of the second laser is four times larger than that in its absence, i.e. three-photon $N(^2D)$ ionization produces three times as many ions as one-photon NO^* ionization. The factor is even larger when one considers that only the $N(^2D_{5/2})$ population is used in this comparison, the Q frequency being set at the shorter wavelength line of the doublet. It therefore seems likely that most of the NO^* predissociates, and in fact the undissociated fraction could be very small, particularly in view of the potential second predissociative pathway, which yields $N(^4S) + O(^3P)$.

Consistent with the view that the NO^* state is strongly predissociated is the fact that the two lasers do not interchange their tasks well, even when their intensities are similar. The line from the QR laser is $\sim 1.3 \text{ cm}^{-1}$ wide, whereas the line from the Q laser is $\sim 0.2 \text{ cm}^{-1}$ wide. Because of the broad predissociated state and the narrow $N(^2D)$ transition width, it makes sense to use the QR laser for NO photodissociation and the Q laser for $N(^2D)$ detection. Reversing these roles results in much reduced signals.

Figures 16 and 17 compare the power dependence of the $N(^2D)$ signals for the situation where $N(^2D)$ from a N_2 discharge is detected with Q and that where $N(^2D)$ from NO photodissociation is produced and detected with QR. In the former case, the three-photon process exhibits a quadratic dependence at low power and becomes linear as the power is increased. This suggests that the one-photon ionization step is saturated at the lowest power measured. For $N(^2D)$ production from NO, an overall five-photon process, the data in Fig. 17 exhibit a P^3 dependence at low power. Presumably, the effect of the two 2-photon processes would result in a P^4 dependence at yet lower powers.

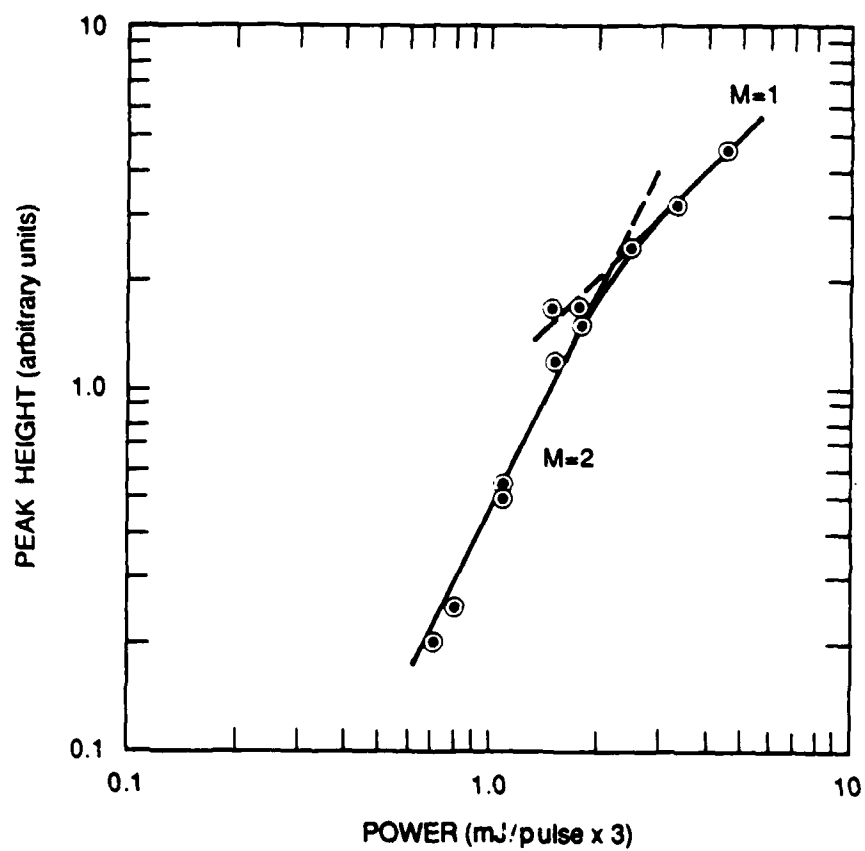


Figure 16. Power dependence of N(²D) from N₂ discharge source [N₂] = 100 mtorr, [He] = 8 torr, QR laser.

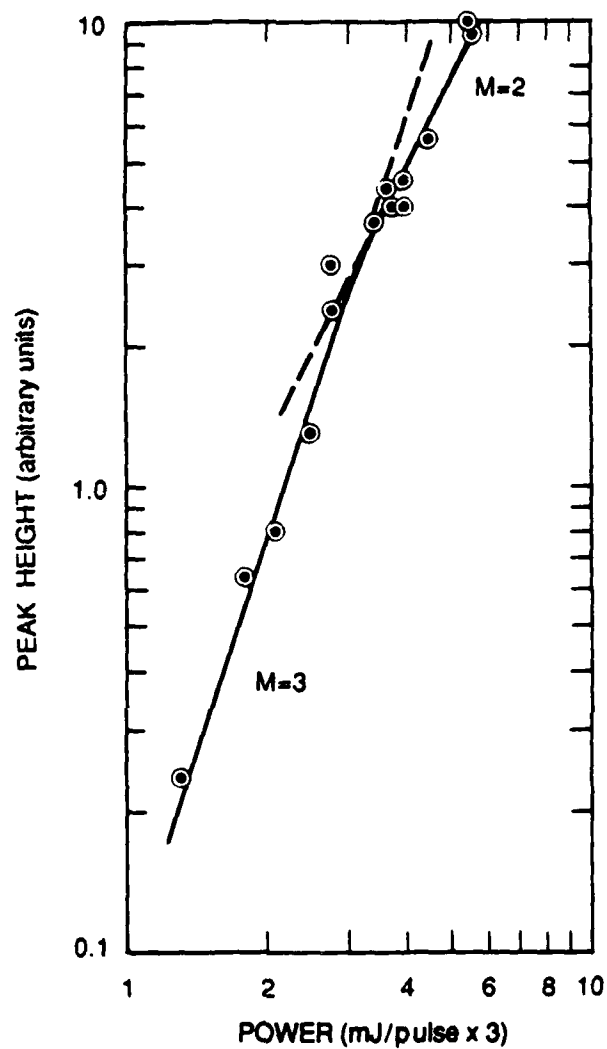
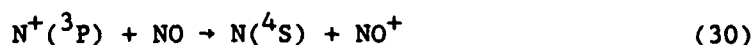


Figure 17. Power dependence of $N(^2D)$ from NO photodissociation [NO] = 5 mtorr, [He] = 5 torr, QR laser.

Figure 18 shows the dependence of the $N(^2D)$ signal on NO density when the Q laser is scanned alone and when it is scanned with the QR laser set at 270.0 nm, the peak of the enhanced signal in Fig. 15. At low pressures, the enhancement is approximately a factor of 20. At high [NO], the enhanced signal falls below its peak value, whereas the signal from the Q laser alone continues to climb, albeit with a decreasing slope.

A possible explanation for the turnover in the enhanced signal is that the rate of charged particle neutralization reactions depends quadratically on both pressure and power. The enhanced signal arises from the production of $N^+(^3P)$, as shown in Fig. 14. At high [NO], rapid conversion to NO^+ will occur according to the reaction



the rate coefficient being $7 \times 10^{-10} \text{ cm}^3 \text{ molecule}^{-1} \text{ s}^{-1}$ (Ref. 87). NO^+ neutralization will then take place by dissociative recombination,



the process becoming increasingly important with increasing pressure. Just such behavior has been observed in two-photon ionization of trimethylamine (Ref. 88) where ion currents exhibit a peak with increasing pressure, and the peak occurs at lower pressures as the laser power is increased. Note that Reaction (31) produces $N(^2D)$ with a yield of 0.76 (Ref. 89), but $N(^2D)$ is not detected in the experiment because it is formed well after the laser pulse.

Although the data of Fig. 18 suggest that the two curves may cross, it is somewhat misleading to compare the curves in this manner. In the first place, an NO^+ ion produced by the Q laser in the absence of the QR laser has a greater chance of escaping neutralization than does one in the highly charged environment created when both lasers are fired. Furthermore, the Q laser is triggered after the QR laser, and thus the environment that the Q laser "sees" may be considerably different from the environment that exists when it is fired alone. In particular, the NO may be considerably depleted in the focal volume after the QR pulse. For these reasons, the difference between the two

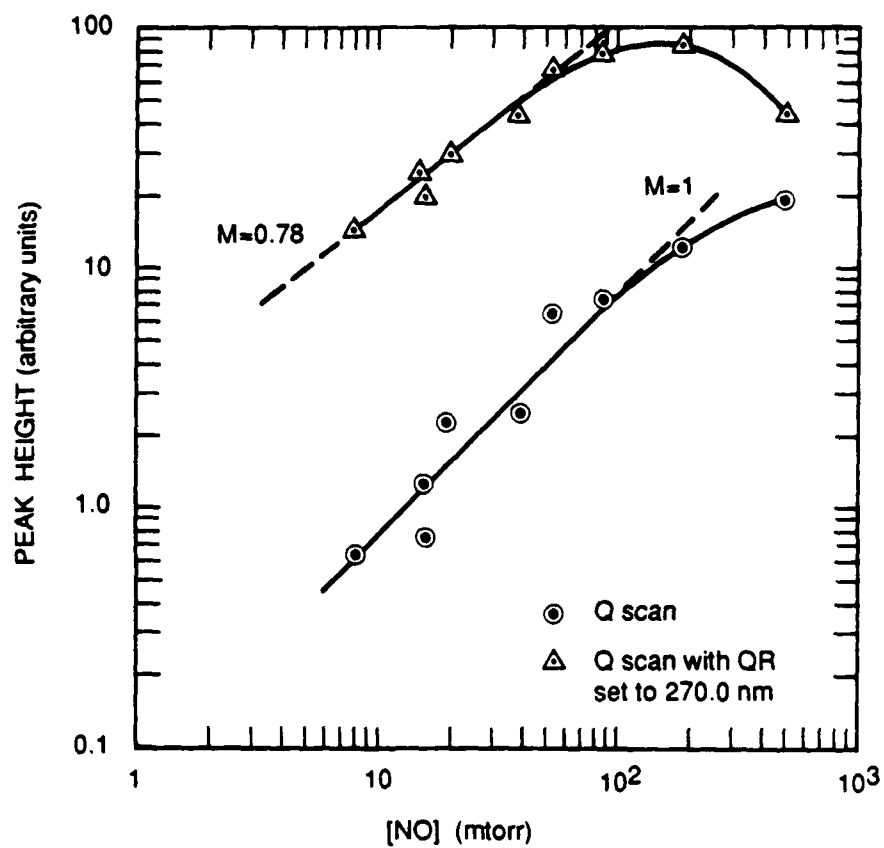


Figure 18. Ion signal versus [NO] Q and Q/QR scans; 1% NO/He, $I_Q = 3$ mJ, $I_{QR} = 3$ mJ.

curves in Fig. 18 should probably not be viewed as the contribution of the QR laser to the total signal.

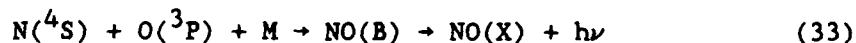
Two-photon production of $N(^2D)$ from NO at 269 nm is obviously more convenient than preparing this atom by vuv photodissociation of N_2O , but it is important to obtain an idea of the amount of $N(^2D)$ made by the two-photon method. This is most easily accomplished by comparing the concentration of photolytically produced $N(^2D)$ with that produced in an N_2 afterglow, for which several measurements have been made. The study of C. L. Lin and F. Kaufman (Ref. 57), which is representative, reports obtaining $[N(^2D)] = 2.4 \times 10^{12}$ molecule cm^{-3} at 3 ms beyond the microwave cavity. The steady state concentration generated by 147-nm irradiation of N_2O is typically in the range 10^7 - 10^8 cm^{-3} .

In this experiment, the discharge-created $N(^2D)$ was measured 11 ms after the discharge, in 10 torr of 1 percent N_2/He , with a Q laser scan. For comparison, 40 mtorr of NO was photodissociated with the QR laser at 270 nm and detected with the Q laser. The ion signal obtained from the photodissociative source was ten times larger than that from the afterglow source, which suggests that on the order of 1 mtorr of $N(^2D)$ is generated by photodissociation of NO. This indicates that, for a two-photon process, the efficiency is quite high.

To determine that the afterglow $N(^2D)$ concentration was as others have claimed, it was measured indirectly. The reaction between $N(^2D)$ and O_2 generates NO (Ref. 57), which in the presence of N-atoms is converted to O-atoms by the following reactions:



Therefore, adding O_2 to an N_2 afterglow should result in production of two O-atoms for every $N(^2D)$ atom. When O- and N-atoms are both present in such a system, emission in the β -band system of NO results as follows (Ref. 90):



Thus, the intensity of the β -band emission upon addition of O_2 should be a measure of the amount of $N(^2D)$ at the addition point, and this intensity can be calibrated by addition of NO instead of O_2 . When NO is added, an equivalent number of O-atoms is produced through Reaction (32), and therefore, at constant $[N(^4S)]$, the number of O-atoms produced by Reaction (19) is absolutely known. The $[N(^4S)]$ is approximately constant because its concentration in the afterglow is ~ 10 -20 mtorr and the small amount removed by NO addition (< 1 mtorr) is small compared to this. The β -band intensity after O_2 addition is expected to plateau, after an initial rise, when the $N(^2D)$ has all been removed. This plateau value then represents the $N(^2D)$ concentration at the titration point. The reaction between ground state N-atoms and O_2 is so slow at room temperature that it does not interfere with the determination (Ref. 91). Furthermore, the steady state density of $N_2(A^3\Sigma_u^+)$, which dissociates O_2 , is typically $\leq 10^{10}$ molecules cm^{-3} , 2-3 orders of magnitude smaller than that of $N(^2D)$ (Ref. 92), and should also have a negligible effect.

Figure 19 shows the behavior of the β -band signal upon O_2 addition. The $O(^3P)$ calibration signal in terms of the ordinate units was found to be 100 units/mtorr. The signal bends over at ~ 25 units, so the conclusion is that the $N(^2D)$ concentration at the addition point is ~ 0.12 mtorr. This is comparable to the values reported by others (Ref. 57). Because the $N(^2D)$ produced from NO two-photon dissociation should be ten times larger (see page 56), the localized $N(^2D)$ concentration appeared to be on the order of 1.2 mtorr.

The lack of a true plateau in Fig. 19 may indicate that there are local sources of $N(^2D)$, i.e., that it is generated indirectly through the recombination energy of N-atoms, as discussed in other contexts (Ref. 85). A spectroscopic comparison over the range 200-450 nm was made of the β -band emission from O_2 addition and that resulting from NO titration. The features in the two spectra were identical and originated principally from NO(B) emission from $v' = 0,3$, as reported in Ref. 90. Emission from $v' = 1,2$ was relatively weak, as was emission from the NO γ -bands. It is therefore evident that the β -band intensity is a measure of the $[N][O]$ product, and, as $[N]$ is constant, $[O]$ is proportional to $I(\beta)$.

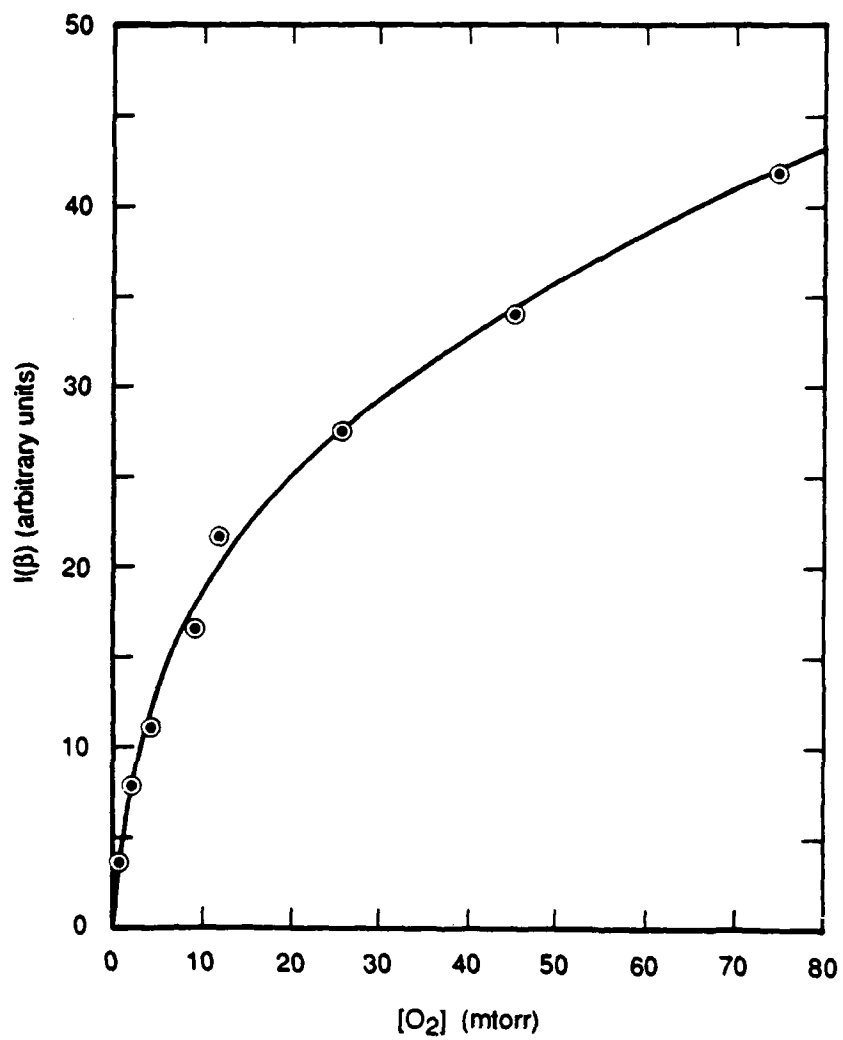


Figure 19. NO β -band intensity versus $[O_2]$ in N_2 afterglow.
Detected wavelength = 360 nm, $[N_2]$ = 200 mtorr, $[HE]$ = 10 torr.

The validity of this technique for obtaining $N(^2D)$ concentrations is confirmed by further experiments using N_2O and CO_2 as the $N(^2D)$ quenchers. These two gases react with $N(^2D)$ to produce NO , as does O_2 (Ref. 57), and in each case, the initial slopes of the plots are compatible with the respective rate coefficients for quenching $N(^2D)$ (Ref. 40). In all these experiments, He was the buffer gas. If Ar is used, very different results are obtained because of the interaction of Ar^* with N_2 and the subsequent N_2^*/O_2 chemistry.

The local $N(^2D)$ concentrations that we have measured for the photodissociative source are higher than those reported for any other production system. However, the volume having this concentration is quite small. The hole made by the focused beam in a metal foil has a diameter of $150\ \mu m$. If $N(^2D)$ is only produced in this region, and the waist length is 1 cm, the active volume is $2.5 \times 10^{-4}\ cm^3$ or less; thus, the number of $N(^2D)$ atoms would be $\leq 8 \times 10^9$.

Although the present system may lead to very interesting spectroscopic and dynamic studies, such a two-laser experiment has significant limitations for kinetics purposes. When the beams are overlapped, an atom need move only $150\ \mu m$ to be undetectable. At a velocity of $5 \times 10^4\ cm/s$, such a move takes place in 300 ns, in which time an atom will suffer few collisions in a low pressure system (the collision time at 1 torr is 100 ns). Thus, signal attenuation results primarily from diffusion, not quenching. A 100-ns delay between the two lasers at 5 torr pressure gave a $1/e$ reduction of the ion signal.

A good photolytic source of $N(^2D)$ has been developed along with a good method for detecting it, but combining the two techniques requires some care. It is interesting to contemplate that when the lasers are not spatially superimposed, it should be possible to perform time-of-flight measurements on $N(^2D)$. At 10 mtorr total pressure, an atom will travel $\sim 5\ mm$ before suffering a collision.

Because multiphoton studies on NO have been popular in recent years, researchers should be aware of this two-photon dissociative channel in the 267-279 nm region: $N(^2D)$ is a very reactive species that might cause unexpected effects.

8.0 $N(^2D)$ MEASUREMENT IN $C_2N_2-O_2$

The final task was to return to the $C_2N_2-O_2$ system to demonstrate the presence of $N(^2D)$ and obtain an idea of its concentration. Figure 20a shows the characteristic $N(^2D)$ signal in a $C_2N_2/O_2/He$ mixture 45 μs after exposure to a pulse of 158-nm radiation. Figure 20b shows the background obtained with the O_2 turned off to demonstrate that a chemical source of $N(^2D)$ is involved. There appears to be a small signal with C_2N_2 alone, which may indicate some direct production of $N(^2D)$, the effect of some impurity O_2 , or other $N(^2D)$ -generating chemistry.

The temporal profile of the $N(^2D)$ signal is shown in Fig. 21. The absolute concentration scale for $N(^2D)$ comes from comparing the $N(^2D)$ signal from the $C_2N_2-O_2$ systems with that obtained from two-photon absorption of NO at 269 nm (as described in Section 7). The uncertainty in the absolute concentration scale may be as large as a factor of two. With the measured laser flux, the C_2N_2 and O_2 concentrations, and known cross sections at 158 nm, the initial concentration of CN radicals can be estimated at $\sim 3 \times 10^{14}$ molecules cm^{-3} and that of O atoms at $\sim 5 \times 10^{13}$ molecules cm^{-3} . The peak $N(^2D)$ density of $\sim 3 \times 10^{12}$ molecules cm^{-3} seems in line with the predictions of earlier computer modeling (which did not include predictions for the specific concentrations calculated above). It was also possible to show that the $N(^2D)$ signal was increased by the addition of argon (the increase was presumably related to reducing diffusional losses of the reactants) and that the $N(^2D)$ signal could be seen when the irradiation wavelength was changed to 193 nm [this wavelength only dissociates the C_2N_2 , which has an absorption cross section of $\sim 10^{-19}$ cm^2 . The oxygen atoms needed for Reaction (14) come from Reaction (13)].

These exciting developments lend further support to the validity of the chemical modeling and suggest the need to perform further calculations for comparison with the results shown in Fig. 21 and those of similar experiments.

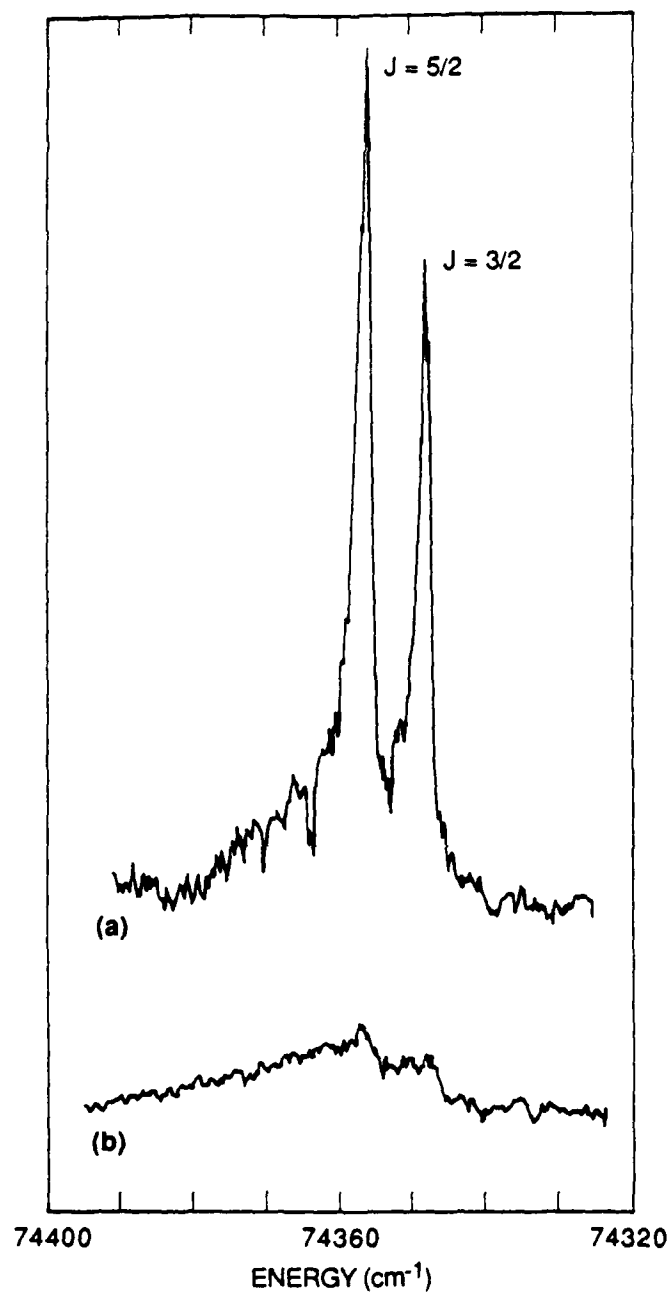


Figure 20. (a) REMPI signal from $N(^2D)$ generated in a $C_2N_2/O_2/He$ mixture 45 μs after a pulse of 158-nm radiation. $C_2N_2 = 30$ mtorr, $O_2 = 10$ mtorr and $He = 3.1$ torr. (b) Background signal with no O_2 .

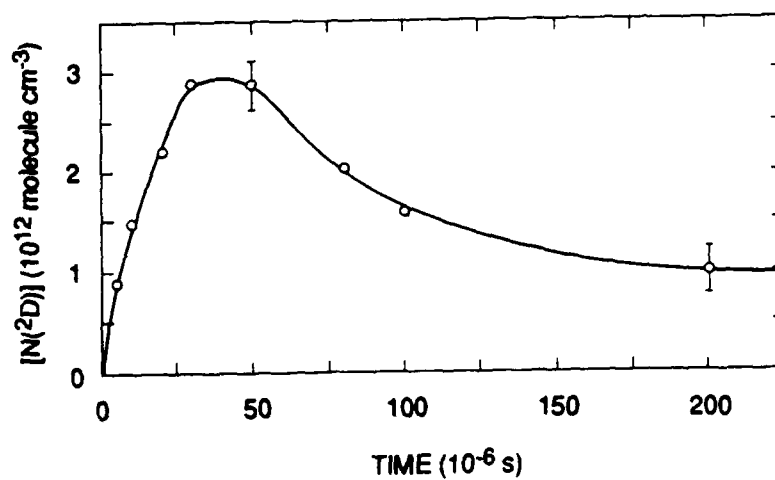
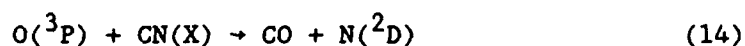


Figure 21. Temporal profile of $N(2D)$ generated in a $C_2N_2/O_2/He$ mixture after a pulse of 158-nm radiation.
 $C_2N_2 = 30$ mtorr, $O_2 = 10$ mtorr, and $He = 3.1$ torr.

9.0 CONCLUSIONS

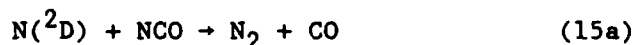
The $C_2N_2-O_2$ system continues to show promise as a chemical source of the metastable nitrogen species $N(^2D)$ and $N_2(A)$. The results to date, in conjunction with expectations from computer modeling, suggest that the basic understanding of the system is correct and that the chemistry provides efficient production of both $N(^2D)$ and $N_2(A^3\Sigma_u^+)$. Although the chemistry is complex, the results suggest that the reaction



is a fast, efficient source of $N(^2D)$; almost two orders of magnitude faster than the reaction



and that the subsequent reaction,



is a fast and efficient source of $N_2(A)$. Further understanding of the detailed kinetics and chemistry in the $C_2N_2-O_2$ system remains a challenge. This system must be better understood before an attempt is made to bridge the gap to the conditions necessary for a chemical laser based on nitrogen.

The REMPI technique has proved a powerful tool for detecting $N(^2D)$: it enabled us to measure rate coefficients that had previously only been estimated, and it permitted investigation of previously inaccessible processes in the chemistry of the $C_2N_2-O_2$ system. Further REMPI investigations and further chemical modeling are needed for a more detailed understanding of this system.

REFERENCES

1. Kompa, K. L., and Pimentel, G. C., "Hydrofluoric Acid Chemical Laser," J. Chem. Phys. 47, 857 (1967).
2. Deutch, T. F., "Molecular Laser Action in Hydrogen and Deuterium Halides," Appl. Phys. Lett. 10, 234 (1967).
3. Hinchey, J. J., "Collision Processes in Chemical Lasers," Appl. Atomic Collision Phys. 3, 191 (1982).
4. Eckstrom, D. J., Edelstein, S. A., Huestis, D. L., Perry, B. E., and Benson, S. W., "Chemiluminescence Studies IV. Pressure-dependent Photon Yields for Ba, Sm, and Eu Reactions with N₂O, O₃, O₂, F₂, and NF₃," J. Chem. Phys. 63, 3828 (1975).
5. Eckstrom, D. J., Edelstein, S. A., Huestis, D. L., Perry, B. E., and Benson, S. W., Stanford Research Institute Report No. MP 74-40, Menlo Park, California (1974).
6. Huestis, D. L., "Theory of Electronic Excitation in Chemical Laser Reactions," in Electronic Transition Lasers, J. I. Steinfeld, ed., MIT Press, Cambridge, Mass. 1976.
7. McDermott, W. E., Pchelkin, N. R., Benard, D. J., and Bousek, R. R., "An Electronic Transition Chemical Laser," Appl. Phys. Lett. 32, 469 (1978).
8. Herbelin, J. M., and Cohen, N., "The Chemical Production of Electronically Excited States in the H/NF₂ System," Chem. Phys. Lett. 20, 605 (1973).
9. Cheah, C. T., and Clyne, M.A.A., "Reactions forming Electronically Excited Free Radicals. Part 2. - Formation of N⁴S, N²D, and N²P Atoms in the H + NF₂ Reaction, and N Atom Reactions," J. Chem. Soc. Faraday Trans. II 76, 1543 (1980).
10. Coombe, R. D., and Pritt, A. T., "Production of Electronically Excited NF by the Reaction of Fluorine Atoms with HN₃," Chem. Phys. Lett. 58, 606 (1978).

11. Cheah, C. T., and Clyne, M.A.A., "Reactions forming Electronically Excited Free Radicals. III: Formation of Excited Molecular States in the $H + NF_2$ Reaction," J. Photochem. **15**, 21 (1981).
12. Hovis, F. E., Whitefield, P. D., Lilienfeld, H. V., and Bradburn, G. R. "Chemical Generation of Electronically Excited N_2 in the $H(D) + NF_2$ Flame," J. Phys. Chem. **92**, 5133 (1988).
13. Piper, L. G., Davis, S. J., Murphy, H. C., Cummings, W. C., Walkauskas, L. P., DeFaccio, M. A., Cowles, L. M., Rawlins, W. T., Marinelli, W. J., and Green, B. D., Conan: Chemistry of Nitrogen-A Nascence, AFWL-TR-86-95, Air Force Weapons Laboratory, Kirtland AFB, New Mexico, January 1988 (unlimited distribution).
14. Davis, S. J. and Coombe, R. D., "Rates of Reactions of the Azide Radical," J. Phys. Chem. **90**, 3260 (1986).
15. Basco, N., "The Reaction of Cyanogen Radicals with Oxygen," Proc. R. Soc. London, Sect. A, **283**, 302 (1965).
16. Schmatjko, K. J., and Wolfrum, J., "Reactions of Molecules in Defined Vibrational States. VI. Energy Distribution in the Reactions $CN(v) + O(^3P)$, O_2 ," Ber. Bunsenges. Phys. Chem. **82**, 419 (1978).
17. Li, X., Sayah, N., and Jackson, W. M., "Laser Measurements of the Effects of Vibrational Energy on the Reactions of CN ," J. Chem. Phys. **81**, 833 (1984).
18. Lichtin, D. A., and Lin, M. C., "Kinetics of CN Radical Reactions with Selected Molecules at Room Temperature," Chem. Phys. **96**, 473 (1985).
19. Whyte, A. R., and Phillips, L. F., "Rate of Reactions of N with $CN(v = 0,1)$," Chem. Phys. Lett. **98**, 590 (1983).
20. Lifshitz, A., and Franklach, M., "Oxidation of cyanogen. II. The Mechanism of the Oxidation," Int. J. Chem. Kinet. **12**, 159 (1980).
21. Setser, D. W., and Thrush, B. A., "Kinetics of Reactions Involving CN Emission. I. General Features of Reactions with Active Nitrogen and Atomic Oxygen," Proc. R. Soc. London, Sect. A **288**, 256 (1965).

22. Setser, D. W., and Thrush, B. A., "Kinetics of Reactions Involving CN Emission. II. The Reaction between Oxygen Atoms and Cyanogen," Proc. R. Soc. London, Sect. A **288**, 275 (1965).
23. Lu, R., Halpern, J. B., and Jackson, W. M., "Photodissociation of C_2N_2 , $ClCN$, and $BrCN$ in a Pulsed Molecular Beam," J. Phys. Chem. **88**, 3419 (1984).
24. Young, R. A., Black, G., and Slanger, T. G., "Vacuum-Ultraviolet Photolysis of N_2O . II. Deactivation of $N_3(A^3\Sigma_u^+)$ and $N_2(B^3\Pi_g)$," J. Chem. Phys. **50**, 303 (1969).
25. Coombe, R. D., Department of Chemistry, University of Denver, Denver, CO 80208, private communication (1985).
26. Black, G. "Reactions of HS with NO and NO_2 at 298 K," J. Chem. Phys. **80**, 1103 (1984).
27. Li, X., Sayah, N., and Jackson, W. M., "A Large Vibrational Enhancement in the Reaction of $CN(v'' = 1,2) + NO$," J. Chem. Phys. **83**, 616 (1985).
28. Cookson, J. L., Hancock, G., and McKendrick, K. G., "Reactions of $CHF(\tilde{X}^1A')$ and $NCO(\tilde{X}^2\Pi)$ Radicals," Ber. Bunsenges Phys. Chem. **89**, 335 (1985).
29. Perry, R. A., "Kinetics of the Reactions of NCO Radicals with H_2 and NO using Laser Photolysis - Laser Induced Fluorescence," J. Chem. Phys. **82**, 5485 (1985).
30. Morrow, T., and McGrath, W. D., "Reactions of 1D and 3P Oxygen Atoms with Cyanogen by Flash Photolysis," Trans. Faraday Soc. **62**, 642 (1969).
31. Hand, C. W. and Hexter, R. M., "Flash Photolysis of Ozone-Cyanogen Mixtures," J. Am. Chem. Soc. **92**, 1828 (1970).
32. Whyte, A. R., and Phillips, L. F., "Rate of Reaction of N with $CN(v=0,1)$," Chem. Phys. Lett. **98**, 590 (1983).
33. Lam, L., Dugan, C. H., and Sadowski, C. M., "The Gas Phase Reactions of CN and NO," J. Chem. Phys. **69**, 2877 (1978).

34. Lifshitz, A. and Frenklach, M. "Oxidation of Cyanogen. II. The Mechanism of the Oxidation," Int. J. Chem. Kinet. 12, 159 (1980).
35. Black, G., Slanger, T. G., St. John, G. A. and Young, R. A., "Vacuum-Ultraviolet Photolysis of N_2O . IV. Deactivation of $N(^2D)$," J. Chem. Phys. 51, 116 (1969).
36. Davenport, J. A., Slanger, T. G., and Black, G., "The Quenching of $N(^2P)$ by $O(^3P)$," J. Geophys. Res. 81, 12 (1976).
37. Schofield, K., "Critically Evaluated Rate Constants for Gaseous Reactions of Several Electronically Excited Species," J. Phys. Chem. Ref. Data 8, 723 (1979).
38. Piper, L. G., Caledonia, G. E., and Kennealy, J. P., "Rate Constants for Deactivation of $N_2(A)_{v'=0,1}$ by O_2 ," J. Chem. Phys. 74, 2888 (1981).
39. Iannuzzi, M. P., and Kaufman, J., "Rate Constants for the Reactions of $N_2(A^3\Sigma_u^+, v=0,1, \text{ and } 2)$ with O_2 ," J. Phys. Chem. 85, 2163 (1981).
40. Piper, L. G., Caledonia, G. E., and Kennealy, J. P., "Rate Constants for Deactivation of $N_2(A^3\Sigma_u^+, v'=0, 1)$ by O ," J. Chem. Phys. 75, 2847 (1981).
41. Hill, R. M., Gutcheck, R. A., Huestis, D. L., Mukherjee, D., and Lorents, D. C., Stanford Research Institute Report No. MP 74-39, Menlo Park, Calif., July 1974.
42. Nadler, I., Rotem, A., and Rosenwaks, S., "Observation of New Bands in the N_2 Herman Infrared System and Kinetic Study of its Formation in a Pulsed-Discharge Apparatus," Chem. Phys. 69, 375 (1982).
43. Clark, W. G., and Setser, D. W., "Energy Transfer Reactions of $N_2(A^3\Sigma_u^+)$. 5. Quenching by Hydrogen Halides, Methyl Halides, and other Molecules," J. Phys. Chem. 84, 2225 (1980).
44. Slanger, T. G., Wood, B. J., and Black, G., "Temperature-Dependent $N_2(A^3\Sigma_u^+)$ Quenching Rate Coefficients," Photochem. 2, 63 (1973).
45. Dunn, O. J., and Young, R. A., "Quenching of $N_2(A^3\Sigma_u^+)$ by O_2 , O , N , and H ," Int. J. Chem. Kinet. 8, 161 (1976).

46. Braun, W., Bass, A. M., Davis, D. D., and Simmons, J. D., "Flash Photolysis of Carbon Suboxide: Absolute Rate Constants for Reactions of $C(^3P)$ and $C(^1D)$ with H_2 , N_2 , CO , NO , O_2 , and CH_4 ," Proc. R. Soc. Sect. A 312, 417 (1969).
47. Baulch, D. L., Drysdale, D. D., Horne, D. G., and Lloyd, A. C., Evaluated Kinetic Data for High Temperature Reactions, Vol. 2, Butterworths, London 1973.
48. Taylor, G. W., and Setser, D. W., "Quenching Rate Constants for $CO(a^3\Pi; v'=0,1,2)$," J. Chem. Phys. 58, 4840 (1973).
49. Ottinger, Ch., Simonis, J., and Setser, D. W., "Spectroscopic Study of Electronic Energy Transfer from Molecular Nitrogen (A) and Carbon Monoxide (a) to Nitric Oxide in a Beam Experiment," Ber. Bunsenges Phys. Chem. 82, 655 (1978).
50. Taherian, M.-R. and Slanger, T. G., Molecular Physics Laboratory, SRI International, Menlo Park, CA 94025, unpublished results.
51. Taherian, M.-R. and Slanger, T. G., " C_2N_2 Photodissociation at 1576 Å. I. $CN(A^2\Pi)$ Radiative Lifetimes, Nascent Distributions, and C_2N_2 Quenching," J. Chem. Phys. 81, 3814 (1984).
52. Taherian, M.-R. and Slanger, T. G., "Quenching of $CN(A^2\Pi, v = 0,1)$ by O_2 , H_2 , N_2 , NO , and CO_2 ," J. Chem. Phys. 82, 2511 (1985).
53. Hayes, G. N., and Oskam, H. J., "Population of $N_2(B^3\Pi_g)$ by $N_2(A^3\Sigma_u^+)$ During the Nitrogen Afterglow," J. Chem. Phys. 59, 1507 (1973).
54. David, S. J., and Coombe, R. D., "The Chemiluminescent Reaction of $N(^4S_u)$ Atoms with Azide Radicals," J. Phys. Chem. 89, 5206 (1985).
55. Safrany, D. R., and Jaster, W., "Reactions of Hydrocarbons with Mixtures of Active Nitrogen and Hydrogen Atoms. II. "Anomalous" Reactions: the Reactions of Cyanogen, Hydrogen Cyanide, and Acetylene," J. Phys. Chem. 72, 3305 (1968).
56. Black, G., Slanger, T. G., St. John, G. A., and Young, R. A., "Vacuum-Ultraviolet Photolysis of N_2O . IV. Deactivation of $N(^2D)$," J. Chem. Phys. 51, 116 (1969).

57. Lin, C. L., and Kaufman, F., "Reactions of Metastable Nitrogen Atoms," J. Chem. Phys. 55, 3760 (1971).
58. Iannuzzi, M. P., and Kaufman, F., "Rates of Some Reactions of $N(^2D$ and 2P) near 300 K," J. Chem. Phys. 73, 4701 (1980).
59. Fell, B., Rivas, I. V., and McFadden, D. L., "Kinetic Study of Electronically Metastable Nitrogen Atoms, $N(^2D_J)$, by Electron Spin Resonance Absorption," J. Phys. Chem. 85, 224 (1981).
60. Black, G., and Jusinski, L. E., "Rate Coefficients for $S(^1D)$ Removal at 300 K," J. Chem. Phys. 82, 789 (1985).
61. Black, G., Jusinski, L. E., and Taherian, M.-R., "Spin Orbit Relaxation of $S(3^3P_O)$," Chem. Phys. Lett. 122, 93 (1985).
62. Black, G., "Branching Ratios for Quenching and Reaction in the Interaction of $S(^1D_2)$ with Various Gases," J. Chem. Phys. 84, 1345 (1986).
63. Black, G., and Jusinski, L. E., "Branching Ratios for $S(3^3P_J)$ and $S(3^1D_2)$ Atom Production in the Photodissociation of CS_2 at 193 nm," Chem. Phys. Lett. 124, 90 (1986).
64. Black, G., "Reactions of HS with NO and NO_2 at 298 K," J. Chem. Phys. 80, 1103 (1984).
65. Brewer, P., van Veen, N., and Bersohn, R., "Two-Photon Induced Fluorescence and Resonance-Enhanced Ionization of Sulfur Atoms," Chem. Phys. Lett. 91, 126 (1982).
66. Black, G., Sharpless, R. L., Slanger, T. G., and Lorents, D. C., "Quantum Yields for the Production of $O(^1S)$, $N(^2D)$, and $N_2(A^3\Sigma_u^+)$ from the Vacuum UV Photolysis of N_2O ," J. Chem. Phys. 62, 4266 (1975).
67. Slanger, T. G., and Black, G., "Quenching of $N(^2D)$ by N_2 and H_2O ," J. Chem. Phys. 64, 4442 (1976).
68. van Veen, N., Brewer, P., Das, P., and Bersohn, R., "Detection of the $a^1\Pi_g(v'=0,1) \rightarrow X^1\Sigma_g^+(v''=0)$ transition in N_2 by Laser-Induced Fluorescence," J. Chem. Phys. 77, 4326 (1982).

69. Pratt, S. T., Dehmer, P. M., and Dehmer, J. L., "Photoelectron Studies of Resonant Multiphoton Ionization of Molecular Nitrogen," J. Chem. Phys. **81**, 3444 (1984).
70. Lofthus, A., and Krupenie, P. H., "The Spectrum of Molecular Nitrogen," J. Phys. Chem. Ref. Data **6**, 113 (1977).
71. Black, G., Slanger, T. G., and St. John, G. A., "Vacuum-Ultraviolet Photolysis of N_2O . IV. Deactivation of $N(^2D)$," J. Chem. Phys. **51**, 116 (1969).
72. Husain, D., Mitra, S. K., and Young, A. N., "Kinetic Study of Electronically Excited Nitrogen Atoms, $N(2^2D_J, 2^2P_J)$, by Attenuation of Atomic Resonance Radiation in the Vacuum Ultraviolet," J. Chem. Soc. Faraday Trans. II **70**, 1721 (1974).
73. Bell, D. D., and Coombe, R. D., "Photodissociation of Chlorine Isocyanate," J. Chem. Phys. **82**, 1317 (1985).
74. Black, G., and Jusinski, L. E., "Multiphoton Production and Detection of $N(^2D)$," Chem. Phys. Lett. **139**, 41 (1987).
75. Bashkin, S., and Stoner, Jr., J. O., Atomic Energy Levels and Grotrian Diagrams, North-Holland/American Elsevier, New York (1975), vol 1.
76. Black, G., Jusinski, L. E., Taherian, M.-R., Slanger, T. G., and Huestis, D. L., "Chemiluminescent Reactions in Photodissociated Cyanogen-Oxygen Mixtures," J. Phys. Chem. **90**, 6842 (1986).
77. Bass, A. M., "Absorption Spectrum of the "Pink" Afterglow of Nitrogen in the Vacuum Ultraviolet," J. Chem. Phys. **40**, 695 (1964).
78. Tanaka, Y., Innes, F. R., Jursa, A. S., and Nakamura, M., "Absorption Spectra of the Pink and Lewis-Rayleigh Afterglows of Nitrogen in the Vacuum-UV Region," J. Chem. Phys. **42**, 1183 (1965).
79. Tanaka, Y., Jursa, A. S., and LeBlanc, F. J., The Threshold of Space, Pergamon Press, Inc., New York, 1957, p 89.
80. Zakheim, D. S., and Johnson, P. M., "Rate Equation Modelling of Molecular Multiphoton Ionization Dynamics," Chem. Phys. **46**, 263 (1980).

81. Godefroid, M., and Froese-Fischer, C., "MCHF-BP Fine-Structure Splittings and Transition Rates for the Ground Configuration in the Nitrogen Sequence," J. Phys. B **17**, 681 (1984).
82. Fraser, M. E., Rawlins, W. T., and Miller, S. M., "Auroral Chemiexcitation and Infrared Branching Ratios for the Fundamental and First Overtone Vibrational Transitions of NO($X^2\Pi$, $v \leq 12$)," Paper SA41B-08, EOS, Trans. Am. Geophys. Union **69**, 419 (1988).
83. Cleary, D. D., "Daytime High-Latitude Rocket Observations of the NO γ, δ , and ϵ Bands," J. Geophys. Res. **91**, 11337 (1986).
84. Jusinski, L. E., Black, G., and Slinger, T. G., "Quenching of N(2D) by Cyanogen," Chem. Phys. Lett. **141**, 58 (1987).
85. Jusinski, L. E., Black, G., and Slinger, T. G., "Resonance-Enhanced Multiphoton Ionization Measurements of N(2D) Quenching by O(3P)," J. Phys. Chem. **92**, 5977 (1988).
86. Slinger, T. G., Bischel, W. K., and Dyer, M. J., "Nascent NO Vibrational Distribution from 2485 Å NO₂ Photodissociation," J. Chem. Phys. **79**, 2231 (1983).
87. Goldan, P. D., Schmeltekopf, A. L., Fehsenfeld, F. C., Schiff, H. I., and Ferguson, E. E., "Thermal Energy Ion-Neutral Reaction Rates. II. Some Reactions of Ionospheric Interest," J. Chem. Phys. **44**, 4095 (1966).
88. Lee, L. C., and Bischel, W. K., "Two-Photon-Ionization Coefficients of Propane, 1-Butene, and Methylamines," J. Appl. Phys. **53**, 203 (1982).
89. Kley, D., Lawrence, G. M., and Stone, E. J., "The Yield of N(2D) Atoms in the Dissociative Recombination of NO⁺," J. Chem. Phys. **66**, 4157 (1977).
90. Young, R. A., and Sharpless, R. L., "Chemiluminescent Reactions Involving Atomic Oxygen and Nitrogen," J. Chem. Phys. **39**, 1071 (1963).
91. Becker, K. H., Groth, W., and Kley, D. C., "The Rate Constant of the Aeronomic Reaction N + O₂," Z. Naturforsch. **A24**, 1280 (1969).
92. Richards, D. S., and Setser, D. W., "Excitation-Transfer Studies of N₂(A³ Σ_u^+) with S Atoms and CS Molecules," Chem. Phys. Lett. **136**, 215 (1987).

BIBLIOGRAPHY

- G. Black and L. E. Jusinski, "Multiphoton Production and Detection of $N(^2D)$," Chem. Phys. Lett. 139, 41 (1987).*
- G. Black, L. E. Jusinski, M -R. Taherian, T. G. Slanger, and D. L. Huestis, "Chemiluminescent Reactions in Photodissociated Cyanogen-Oxygen Mixtures," J. Phys. Chem. 90, 6843 (1986).*
- G. Black, L. E. Jusinski, and T. G. Slanger, "Quenching of $N(^2D)$ by Cyanogen," Chem. Phys. Lett. 141, 58 (1987).*
- G. Black, T. Nishiya, H. Shinohara, N. Nishi, and I. Hanazaki, "REMPI Studies in the Lewis-Rayleigh Afterglow of Nitrogen," Chem. Phys. Lett. 142, 409 (1987).**
- L. E. Jusinski, G. E. Gadd, G. Black, and T. G. Slanger, " $N(^2D)$ Production by 2-Photon NO Photodissociation," submitted to J. Chem. Phys. (1988).*

* These papers resulted from this project.

** Although the initial observations were made on this project, major support was also provided by the Institute for Molecular Science, Okazaki, Japan, while one of the authors (G. Black) was a Visiting Professor (April-September, 1987).